The Plant Cell, Vol. 26: 1729–1745, April 2014, www.plantcell.org

Clathrin and Membrane Microdomains Cooperatively Regulate RbohD Dynamics and Activity in *Arabidopsis*[C][W]

Huaiqing Hao,[a,1] Lusheng Fan,[a,1] Tong Chen,[a] Ruili Li,[b,c] Xiaojuan Li,[b,c] Qihua He,[d] Miguel A. Botella,[e] and Jinxing Lin[b,c,2]

[a] Key Laboratory of Plant Resources, Institute of Botany, Chinese Academy of Sciences, Beijing 100093, China
[b] Key Laboratory of Plant Molecular Physiology, Institute of Botany, Chinese Academy of Sciences, Beijing 100093, China
[c] College of Biological Sciences and Biotechnology, Beijing Forestry University, Beijing 100083, China
[d] Peking University Health Science Center, Beijing 100191, China
[e] Departamento de Biología Celular, Genética, y Fisiología, Universidad de Málaga, 29071 Malaga, Spain

Arabidopsis thaliana **respiratory burst oxidase homolog D (RbohD) functions as an essential regulator of reactive oxygen species (ROS). However, our understanding of the regulation of RbohD remains limited. By variable-angle total internal reflection fluorescence microscopy, we demonstrate that green fluorescent protein (GFP)-RbohD organizes into dynamic spots at the plasma membrane. These RbohD spots have heterogeneous diffusion coefficients and oligomerization states, as measured by photobleaching techniques. Stimulation with ionomycin and calyculin A, which activate the ROS-producing enzymatic activity of RbohD, increases the diffusion and oligomerization of RbohD. Abscisic acid and flg22 treatments also increase the diffusion coefficient and clustering of GFP-RbohD. Single-particle analysis in *clathrin heavy chain2* mutants and a *Flotillin1* artificial microRNA line demonstrated that clathrin- and microdomain-dependent endocytic pathways cooperatively regulate RbohD dynamics. Under salt stress, GFP-RbohD assembles into clusters and then internalizes into the cytoplasm. Dual-color fluorescence cross-correlation spectroscopy analysis further showed that salt stress stimulates RbohD endocytosis via membrane microdomains. We demonstrate that microdomain-associated RbohD spots diffuse at the membrane with high heterogeneity, and these dynamics closely relate to RbohD activity. Our results provide insight into the regulation of RbohD activity by clustering and endocytosis, which facilitate the activation of redox signaling pathways.**

INTRODUCTION

Reactive oxygen species (ROS) play crucial roles in immune functions in both plants and animals; for example, in animals, phagocyte oxidase produces superoxide in white blood cells (Hopps et al., 2009). In plants, the respiratory burst oxidase homolog (rboh) proteins were identified based on their sequence similarity to the mammalian 91-kD glycoprotein subunit of phagocyte oxidase (gp91^{phox}) or NADPH oxidase 2 (NOX2) (Keller et al., 1998). Rboh proteins have cytosolic FAD and NADPH binding domains and six membrane-spanning domains. They transfer electrons from cytosolic NADPH or NADH to apoplastic oxygen, leading to the production of apoplastic superoxide (Sagi and Fluhr, 2006). Sequence analysis identified 10 members of the *Rboh* gene family in *Arabidopsis thaliana* (Torres and Dangl, 2005). However, unlike the mammalian gp91^{phox}/NOX2 protein, plant Rboh proteins have an additional hydrophilic N-terminal region, containing two EF-hands and a phosphorylation domain (Torres, 2010). Functional studies have shown that Ca^{2+}-dependent phosphorylation and interaction with members of RhoGTPases of plants regulate the activity of these proteins (Ogasawara et al., 2008; Takeda et al., 2008; Kimura et al., 2012). Rboh proteins function in a plethora of processes, such as pathogen resistance, abiotic stress tolerance, and signal transduction (Galletti et al., 2008; Monshausen et al., 2009). The Rboh family members differ in their expression and distribution in tissues and organs (Groom et al., 1996; Müller et al., 2009; Suzuki et al., 2011). Also, the specific expression of the different Rboh members conditions their function in vivo. For example, *RbohC* is specifically expressed in trichoblasts and has a major role in the focal production of ROS leading to the polarized growth of root hairs. *RbohD* shows the highest expression of the ten *Rboh* genes (Suzuki et al., 2011) and functions in abscisic acid–induced stomatal closure, flagellin-induced immune responses, and salt acclimation, all via ROS production (Torres et al., 2002; Pogány et al., 2009; Xie et al., 2011). Although the involvement of *RbohD* in protecting plants from biotic and abiotic stresses has been extensively studied and factors that regulate RbohD activity have been identified, the manner in which it exerts its role in the plasma membrane and its dynamics in relation to the membrane microdomains in plants remain unclear.

The lateral organization of the cell membrane critically influences the kinetic properties of membrane proteins. However, traditional biochemical techniques with low spatial and temporal resolution cannot examine the dynamics of membrane proteins in living cells. Thus, revealing the spatial and temporal details of membrane proteins and determining their state and dynamics require analytical tools with high temporal and spatial resolution. In this study, we

[1] These authors contributed equally to this work.
[2] Address correspondence to linjx@ibcas.ac.cn.
The author responsible for distribution of materials integral to the findings presented in this article in accordance with the policy described in the Instructions for Authors (www.plantcell.org) is: Jinxing Lin (linjx@ibcas.ac.cn).
[C] Some figures in this article are displayed in color online but in black and white in the print edition.
[W] Online version contains Web-only data.
www.plantcell.org/cgi/doi/10.1105/tpc.113.122358

used dual-color variable-angle total internal reflection fluorescence microscopy (VA-TIRFM) and fluorescence correlation/cross-correlation spectroscopy (FCS/FCCS) to quantitatively characterize the localization and dynamics of green fluorescent protein (GFP)-RbohD in living cells. We found that GFP-RbohD primarily localizes at the plasma membrane and forms discrete foci at the cortex. Ca^{2+}, phosphorylation, and NaCl, known effectors of NADPH oxidase activity, affect the diffusion coefficient and endocytosis of GFP-RbohD. In addition, we provide evidence that clathrin- and microdomain-dependent endocytic pathways cooperatively regulate the dynamic partitioning and internalization of GFP-RbohD.

RESULTS

Dynamic Behavior and Assembly State of GFP-RbohD at the Plasma Membrane

To examine the dynamic behavior of RbohD at the plasma membrane in *Arabidopsis*, we generated transgenic plants expressing an N-terminal GFP fused to *RbohD* under the control of the native *RbohD* promoter. We confirmed that the GFP-RbohD protein retains function by complementing the *rbohD* mutant phenotype for plant growth (Figures 1A to 1C) and ROS production (Figures 1D to 1F). Laser scanning confocal microscopy of the seedlings revealed that GFP-RbohD was expressed in most tissues (Supplemental Figure 1A), consistent with previous reports and the available microarray data (Torres et al., 1998) and with the proposed housekeeping role for RbohD. GFP-RbohD targeted to the plasma membrane of epidermal cells, with high expression in the leaves, stomata, hypocotyls, and roots (Figures 1G to 1I). We further analyzed the distribution of fluorescent signals of GFP-RbohD and the membrane marker FM4-64. Most FM4-64 fluorescence colocalized with the green GFP-RbohD fluorescence at the plasma membrane. FM4-64 internalization increased with incubation time, and we also observed some intracellular colocalization of GFP-RbohD with FM4-64 (Figure 1J). To determine whether plasma membrane localization of GFP-RbohD depends on vesicle trafficking, we next used the vesicle transport inhibitor brefeldin A (BFA), which can block vesicle transport from endoplasmic reticulum to Golgi by

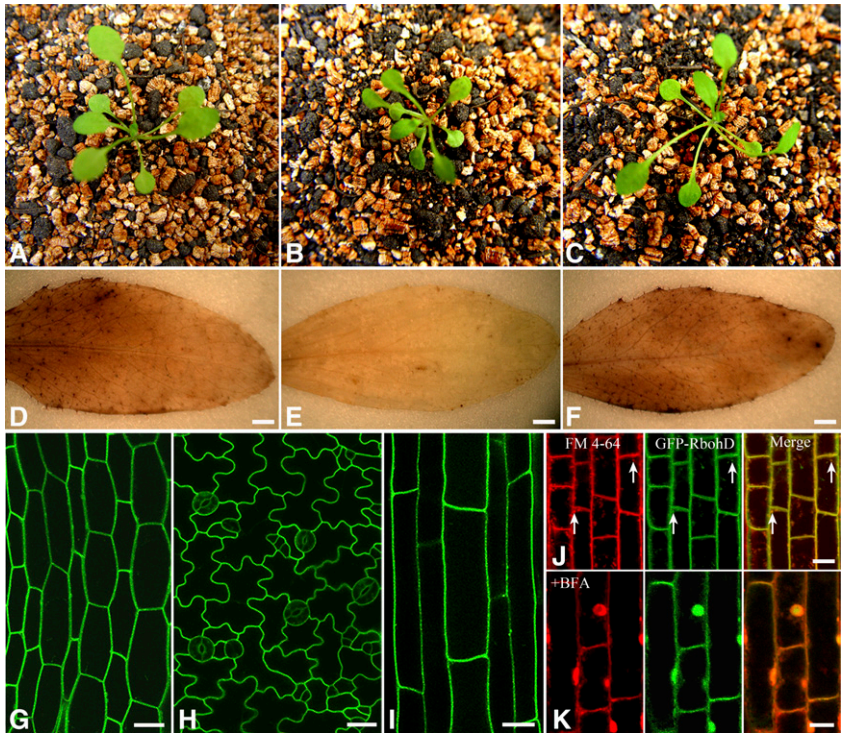

Figure 1. Distribution and Localization of GFP-RbohD in *Arabidopsis* Seedlings.

(A) to **(C)** Phenotypes of wild-type **(A)**, *rbohD* **(B)**, and *pRbohD:GFP-RbohD* transgenic seedlings in the *rbohD* background **(C)**.
(D) to **(F)** H_2O_2 production in leaves of wild-type **(D)**, *rbohD* **(E)**, and *pRbohD:GFP-RbohD* transgenic seedlings in the *rbohD* background **(F)** was visualized using 3,3′-diaminobenzidine. Bars = 1 mm.
(G) to **(I)** Confocal images of the expression of GFP-RbohD in *Arabidopsis* seedlings. Micrographs show that GFP-RbohD was localized mainly at the plasma membrane in *Arabidopsis* hypocotyls **(G)**, leaf epidermal cells **(H)**, and root cells **(I)**. Bars = 20 μm.
(J) Roots of *Arabidopsis* seedlings were stained with endocytic tracer FM4-64 (3 μM) and then observed after incubation for 10 min. In control cells, colocalization of GFP-RbohD and FM4-64 was observed at the plasma membrane and the intracellular structure (white arrow). FM4-64 labeling (red), GFP-RbohD (green), merged channels (yellow).
(K) When roots were pretreated with BFA (50 μM) for 1 h and then incubated with 50 μM BFA and 5 μM FM4-64 for 30 min, GFP-RbohD colocalized with FM4-64 in the BFA compartment. For all analyses, the results shown are representative of >15 independent samples. Bars = 10 μm **(J)** and **(K)**.

interfering with COP I vesicle formation, resulting in the accumulation of plasma membrane proteins in BFA compartments. BFA treatment caused GFP-RbohD to accumulate in the BFA compartment, where it colocalized with FM4-64 (Figure 1K). To rule out the possibility that the appearance of GFP-RbohD in the intracellular FM4-64–positive vesicles was due to newly synthesized protein, we further investigated the localization of GFP-RbohD in the presence of the specific protein synthesis inhibitor cycloheximide (CHX). After pretreatment with CHX for 30 min, the transgenic seedlings were incubated with FM4-64. We observed colocalization of FM4-64 and GFP-RbohD in the cytoplasm (Supplemental Figure 1B). In addition, FM4-64 and GFP-RbohD still accumulated in the BFA compartment in the presence of CHX (Supplemental Figure 1C). These results indicate that constitutive endocytic turnover is likely an important process for maintaining GFP-RbohD at the plasma membrane.

We then used VA-TIRFM to monitor the in vivo dynamics of RbohD at the plasma membrane. This technique allows us to image the plant cell cortex at high resolution and with a high signal-to-noise ratio (Li et al., 2011; Malinsky et al., 2013). In the hypocotyl epidermal cells of the seedlings, GFP-RbohD fluorescent foci formed discreet spots, instead of distributing uniformly in the plasma membrane (Figure 2A). Although we observed a few immobile spots, most of the spots were mobile at the plasma membrane (Supplemental Movie 1 and Supplemental Data Set 1). GFP-RbohD spots exhibited various mobile behaviors in the focal plane of the cell cortex, and most moved within the imaging plane before disappearing (Figure 2B). Some spots with high fluorescence intensity disappeared after long-duration residence at the plasma membrane. Other spots first appeared with low fluorescence intensity; after reaching peak intensity, their fluorescence then decreased and the spots disappeared (Figure 2C). The kymograph also shows the turnover of single GFP-RbohD spots (Figure 2D). We further investigated the dynamic properties of GFP-RbohD at the plasma membrane by determining the lateral mobility of GFP-RbohD using single-particle tracking and a linear fit of mean square displacement (MSD) versus time plots. We used the rolling ball method to subtract the background of the images and plotted the diffusion coefficients on histograms and then fitted the data using the Gaussian function, in which we defined the Gaussian peaks (indicated as $\hat{G}$) as the characteristic diffusion coefficients. In control seedlings, we found that $\hat{G}$ was $2.26 \pm 0.19 \times 10^{-2}$ $\mu m^2/s$, with most of the diffusion coefficients ranging from 3.16×10^{-3} to 1.8×10^{-1} $\mu m^2/s$ (Figure 3A), indicating a highly heterogeneous diffusion mobility for GFP-RbohD at the plasma membrane. In addition, when we analyzed the raw images without subtracting the background, we found that the diffusion coefficient of GFP-RbohD was $2.32 \pm 0.13 \times 10^{-2}$ $\mu m^2/s$, similar to that of the processed images (Supplemental Figure 1D).

To evaluate the oligomerization state of GFP-RbohD at the plasma membrane, we performed calibration experiments examining purified GFP monomers by VA-TIRFM to determine the fluorescence intensity of a single GFP-RbohD molecule. Fluorescence intensities of the purified GFP monomers exhibited a unimodal distribution with a peak intensity of ~78 counts (Supplemental Figure 2). Furthermore, we used VA-TIRFM to image the fluorescence intensity distribution

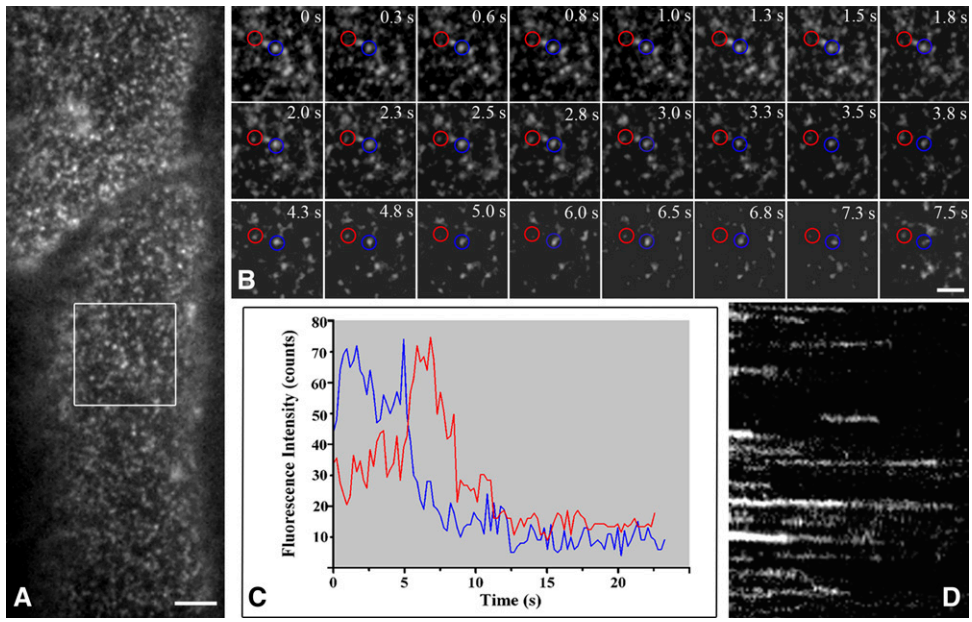

Figure 2. Dynamics of GFP-RbohD Foci at the Plasma Membrane in *Arabidopsis* Seedlings.

(A) A single-particle image of diffraction-limited spots of GFP-RbohD at the plasma membrane in living cells imaged with VA-TIRFM.
(B) Dynamic analysis using a time series of the boxed area in **(A)**. Red and blue circles indicate the fluorescent spots analyzed in **(C)**.
(C) Fluorescence intensity profile of the various foci indicated in **(B)**.
(D) The corresponding kymograph from a representative time series recorded for 15 s.
Bars = 5 μm **(A)** and 2 μm **(B)**.

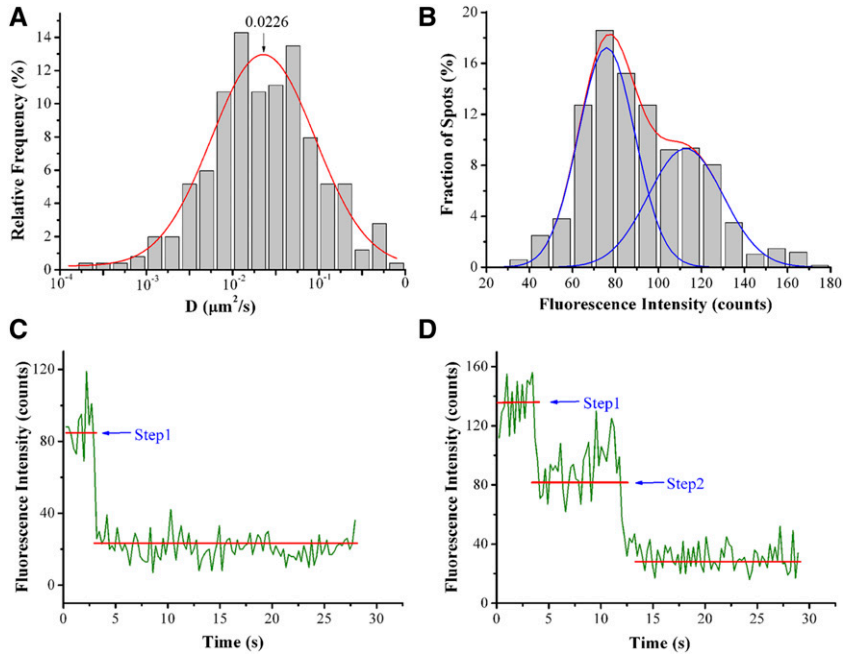

Figure 3. Diffusion Coefficient Distribution, Fluorescence Intensity, and Oligomeric State Analysis of GFP-RbohD Foci at the Plasma Membrane.

(A) Distribution of diffusion coefficients (D) of GFP-RbohD spots on the epidermal cell plasma membrane (n = 526 spots).
(B) Distribution of fluorescence intensities of GFP-RbohD spots in living cells (n = 688 spots).
(C) Time courses of GFP emission after background correction, showing one-step bleaching.
(D) Time courses of GFP emission after background correction, showing two-step bleaching. The amplitude of each step was similar to that of single purified GFP molecules observed on cover slips (Supplemental Figure 2).

of GFP-RbohD particles in living cells. The fluorescence intensities were broadly distributed, with most in the range of 50 to 140 counts, which corresponds to one or two GFP molecules (Figure 3B). To further investigate the number of GFP-RbohD molecules in individual spots, we used single-molecule photobleaching, as previously described (Ji et al., 2008). To reduce signal fluctuation due to the diffusion of GFP-RbohD in living-cell membranes, we performed photobleaching in fixed seedlings. The number of bleaching steps ranged from one to two (Figures 3C and 3D), indicating that GFP-RbohD spots include a mixture of monomers and dimers at the plasma membrane.

Regulators of RbohD Activity Affect Its Dynamics at the Plasma Membrane

Ca^{2+} binding and phosphorylation synergistically activate the enzymatic activity of RbohD (Ogasawara et al., 2008; Kimura et al., 2012). Thus, we investigated whether these factors also affect the lateral diffusion of RbohD at the plasma membrane. We first analyzed the effect of diphenyleneiodonium (DPI), a well-known NADPH inhibitor, on the lateral mobility of GFP-RbohD. DPI treatment caused a significant decrease in $\hat{G}$, from 2.26 $\pm$ 0.19 $\times$ 10^{-2} $\mu m^2/s$ in control conditions to 1.68 $\pm$ 0.08 $\times$ 10^{-2} $\mu m^2/s$ ($P < 0.01$) in GFP-RbohD seedlings (Figure 4A; Supplemental Movie 2 and Supplemental Data Set 1). In addition, DPI caused the dimerization state of GFP-RbohD to decrease from 28% in control to 24% (Figure 4D), indicating that DPI may exert a specific effect on the dynamics of GFP-RbohD. We then compared the dynamic behavior of GFP-RbohD and GFP-Lti6a (an internal marker of the plasma membrane) at the plasma membrane in the presence of DPI. Like GFP-RbohD, GFP-Lti6a also formed distinct spots at the plasma membrane (Supplemental Figure 3A). The diffusion coefficient of GFP-Lti6a ranged from 5.62 $\times$ 10^{-3} $\mu m^2/s$ to 3.15 $\times$ 10^{-1} $\mu m^2/s$, with a $\hat{G}$ value of 2.43 $\pm$ 0.11 $\times$ 10^{-2} $\mu m^2/s$ (Supplemental Figure 3B). We further examined the distribution of fluorescence intensity of GFP-Lti6a, which ranged from 120 to 360 counts (Supplemental Figure 3C). We found no significant change in the diffusion coefficient of GFP-Lti6a in cells treated with DPI, and the $\hat{G}$ value was 2.22 $\pm$ 0.10 $\times$ 10^{-2} $\mu m^2/s$ ($P > 0.05$) (Supplemental Figure 3D), indicating that DPI specifically affected the mobility of GFP-RbohD. We also found that increasing Ca^{2+} influx through the plasma membrane, using the Ca^{2+} ionophore ionomycin, caused fluorescence intensities of GFP-RbohD spots to skew to higher values (Figure 4B; Supplemental Movie 3 and Supplemental Data Set 1). In addition to the increase in the diffusion coefficient, from 2.26 $\pm$ 0.19 $\times$ 10^{-2} $\mu m^2/s$ in the control to 4.10 $\pm$ 0.30 $\times$ 10^{-2} $\mu m^2/s$ (Figure 4C), increased intracellular Ca^{2+} levels also caused an increase in the dimerization state of GFP-RbohD to 76% ($P < 0.01$; Figure 4D). However, in the presence of ionomycin, both the diffusion coefficient and intensity of GFP-Lti6a spots showed no significant changes (Supplemental Figures 3E and 3F).

We then investigated the effect of phosphorylation on the dynamics of GFP-RbohD using the Ser/Thr protein phosphatase inhibitor calyculin A and the general kinase inhibitor K-252a.

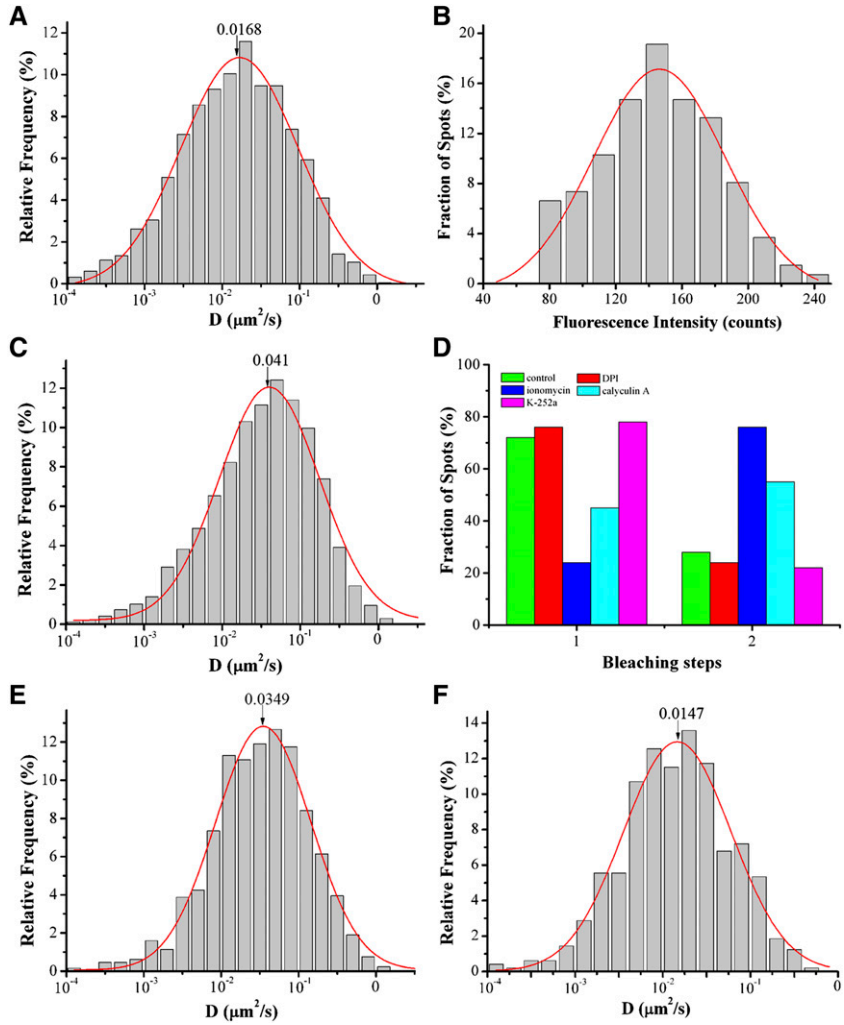

Figure 4. Effects of DPI, Ionomycin, Calyculin A, and K-252a on GFP-RbohD Foci Dynamics at the Plasma Membrane.

(A) Distribution of GFP-RbohD spot diffusion coefficients (labeled D) after DPI treatment (n = 634 spots). (The number indicates the $\hat{G}$ value).
(B) Distribution of GFP-RbohD spot fluorescence intensities in living cells in the presence of ionomycin (n = 445 spots).
(C) Distribution of GFP-RbohD diffusion coefficients on the epidermal cell plasma membrane after treatment with ionomycin (n = 595 spots).
(D) Frequency of one-step and two-step bleaching events for GFP-RbohD without (control, n = 431 spots) and with DPI (n = 415 spots), ionomycin (n = 467 spots), calyculin A (n = 505 spots), or K-252a (n = 503 spots) treatment.
(E) Distribution of GFP-RbohD diffusion coefficients on the epidermal cell plasma membrane after treatment with calyculin A (n = 501 spots).
(F) Distribution of GFP-RbohD diffusion coefficients after treatment with K-252a (n = 489 spots).

Calyculin A caused an increase in both the diffusion coefficient of GFP-RbohD, to 3.49 $\pm$ 0.13 $\times$ 10^{-2} $\mu m^2/s$ (Figure 4E; Supplemental Movie 4 and Supplemental Data Set 1), and its dimerization state, to 55% ($P < 0.05$; Figure 4D). By contrast, the diffusion coefficient and intensity of GFP-Lti6a spots did not change significantly in seedlings treated with calyculin A (Supplemental Figures 3G and 3H). In contrast to calyculin A, K-252a caused a reduction in the diffusion coefficient to 1.47 $\pm$ 0.10 $\times$ 10^{-2} $\mu m^2/s$ (Figure 4F) and the dimerization state to 22% (Figure 4D). However, K-252a had no significant effect on the diffusion coefficient of GFP-Lti6a (Supplemental Figure 3I). These results suggest that Ca^{2+} and phosphorylation, the key regulators of NADPH oxidase activity, also affect the lateral mobility of GFP-RbohD, indicating a close relationship between RbohD enzymatic activity and protein dynamics at the plasma membrane.

As *RbohD* plays an important role in abscisic acid (ABA) responses, we used VA-TIRFM to examine the effects of ABA on the dynamics of GFP-RbohD. ABA induced an increase in the mobility of GFP-RbohD, and the diffusion coefficient increased to 5.32 $\pm$ 0.29 $\times$ 10^{-2} $\mu m^2/s$ (Supplemental Figure 4A, Supplemental Movie 5, and Supplemental Data Set 1). The distribution of GFP-RbohD protein intensity also skewed to higher values, which ranged from 80 to 200 counts (Supplemental Figure 4B), and the number of dimers increased to 75% (Supplemental Figure 4E). In addition, flg22

increased the mobility and intensity of GFP-RbohD, as compared with the control. In the presence of flg22, the diffusion coefficient increased to 4.65 ± 0.41× 10^{-2} μm²/s (Supplemental Figure 4C, Supplemental Movie 6, and Supplemental Data Set 1). The intensity of GFP-RbohD ranged from 100 to 210 counts Supplemental Figure 4D), and the number of dimers increased to 83% (Supplemental Figure 4E). These results further indicated that both ABA and flg22 can increase RbohD mobility and induce its clustering at the plasma membrane.

Endocytosis of RbohD Depends on the Clathrin-Mediated Endocytic Pathway

Endocytosis plays an important role in controlling the internalization of nutrients and the composition of the plasma membrane. Clathrin-mediated endocytosis has been extensively characterized (Mayor and Pagano, 2007) and clathrin-coated pits facilitate the diffusion of plasma membrane proteins (Orr et al., 2005; Xiao et al., 2008b). Tyrphostin A23 (TyrA23), which inhibits mammalian AP-2 binding of endocytic cargo, inhibits clathrin-mediated endocytosis in mammalian and plant cells (Dhonukshe et al., 2007; Konopka et al., 2008). Thus, we investigated whether TyrA23 affects GFP-RbohD dynamics. The results showed that TyrA23 not only increased the number of GFP-RbohD spots but also caused an increase in the size and fluorescence intensity of the spots (Figure 5A; Supplemental Figure 5). In contrast, the diffusion coefficient of GFP-RbohD spots decreased, mostly in the range 1× 10^{-3} to 1.0 × 10^{-1} μm²/s, and Ĝ was 1.54 ± 0.93 × 10^{-2} μm²/s, markedly lower than the control (Figure 5B; Supplemental Movie 7 and Supplemental Data Set 1). To further examine the effects of the clathrin-dependent pathway in the internalization of RbohD, we crossed GFP-RbohD and *chc2-1*, a clathrin heavy-chain (CHC) mutant. As shown in Figure 5C, numerous GFP-RbohD spots accumulated at the membrane in the mutant, and some of the spots clustered into large particles. Additionally, the lateral mobility of GFP-RbohD also decreased significantly, to a Ĝ of 1.95 ± 0.10 × 10^{-2} μm²/s (Figure 5D). We further analyzed the effects of Tyrphostin A51 (TyrA51), the inactive analog of TyrA23, and found that TyrA51 had no significant effect on the distribution and dynamics of GFP-RbohD (Figure 5E, F). In seedlings treated with TyrA51, the diffusion coefficients of RbohD ranged from 5.62 ×10^{-3} μm²/s to 1.78 ×10^{-1} μm²/s, with a Ĝ value of 2.30 ± 0.09 ×10^{-2} μm²/s (Figure 5F). We also found that TyrA51 did not affect the size, fluorescence intensity, or density of GFP-RbohD spots (Supplemental Figures 5 and 7A).

To further address the role of clathrin in RbohD trafficking in plant cells, we generated transgenic plants that expressed an mCherry-tagged *RbohD* translational fusion under the control of the native promoter and evaluated the colocalization of RbohD and clathrin. We used dual-color VA-TIRFM to image seedlings coexpressing mCherry-RbohD and CLC-GFP. To investigate cortical mCherry-RbohD and CLC-GFP dynamics, we chose spots in which both mCherry-RbohD and CLC-GFP were present and determined their codiffusion at the membrane. For quantification, we considered the particles to codiffuse when at least one pixel of their fluorescence signals overlapped during at least five frames, with an interval of 200 ms, as previously reported (Espenel et al., 2008). We found that mCherry-RbohD colocalized with CLC-GFP and codiffused away from the focus gradually, indicating that RbohD internalization associates with the clathrin-dependent pathway (Figures 6A to 6D). We also made more precise calculations by tracking the trajectories of these spots according to the method reported previously (Koyama-Honda et al., 2005). These spots codiffused at the plasma membrane for 6.6 s and kept their distance within 100 nm to each other (Figure 6E). To quantify the degree of colocalization, we calculated the protein proximity index (PPI) (Wu et al., 2010; Zinchuk et al., 2011). PPI is a quantitative measure of the colocalization of proteins, which can give a value between 0 (0% colocalization) and 0.96 ± 0.03 (100% colocalization). Figure 6F shows a 3D plot of the cross-correlation of mCherry-RbohD and CLC-GFP as a function of pixel shift. A sharp peak at the zero pixel shift that decays abruptly by moving the image in the *x* and *y* axes, further supporting specific colocalization. The mean protein proximity value was 0.54 ± 0.1, which further confirmed the specific RbohD and CLC association in the cell cortex.

Membrane Microdomains Contribute to the Localization and Internalization of GFP-RbohD

Sterol- and sphingolipid-enriched membrane microdomains may modulate the localization and activity of certain membrane proteins (Feraru and Friml, 2008). For example, membrane microdomains affect NOX-dependent ROS signaling in *Picea meyeri* pollen tube growth (Liu et al., 2009). Furthermore, a previous plant proteomics analysis identified RbohD in the detergent-resistant membrane fraction (Morel et al., 2006). Therefore, we investigated the role of membrane microdomains in GFP-RbohD dynamics using the sterol-disrupting agent methyl-β-cyclodextrin (mβCD). External application of mβCD resulted in redistribution of GFP-RbohD into small clusters with larger sizes (Figures 7A and 7B) and an increased fluorescence intensity (Supplemental Figure 5). Interestingly, mβCD treatment induced changes in the distribution of the diffusion coefficients into two subpopulations, one of which exhibited a diffusion coefficient similar to control cells, and the other with slower diffusion (3 × 10^{-4} to 3 × 10^{-3} μm²/s; Figure 7C; Supplemental Movie 8 and Supplemental Data Set 1). These results imply that sterol-based membrane microdomains affect the localization and dynamics of GFP-RbohD. To further investigate the role of these microdomains in the regulation of RbohD, we performed parallel experiments by introducing GFP-RbohD into the sterol-deficient mutant *dry2/sqe1-5*. *dry2/sqe1-5* is a hypomorphic allele of *SQUALENE EPOXIDASE1* (*SQE1*), which functions in the synthesis of sterols in plant development and shows very low ROS production due to mislocalization of NADPH oxidases (Posé et al., 2009). As previously reported, GFP-RbohD was mainly confined to the plasma membrane in control seedlings (Figures 7D to 7F). However, we observed faint and discontinuous GFP-RbohD fluorescence in *dry2/sqe1-5* seedlings (Figures 7G and 7H). Additionally, some GFP-RbohD spots were located near the membrane and in the cytoplasm (Figure 7I). These findings indicated a close relationship between GFP-RbohD localization and membrane microdomains.

We further examined the relationship between RbohD and membrane microdomains by analyzing the colocalization of RbohD with the membrane microdomain marker Flotillin1 (Flot1) (Borner et al., 2005), which is involved in a clathrin-independent endocytosis pathway in plant cells (Li et al., 2012). Under dual-color VA-TIRFM, we found that both mCherry-RbohD and GFP-Flot1 foci formed

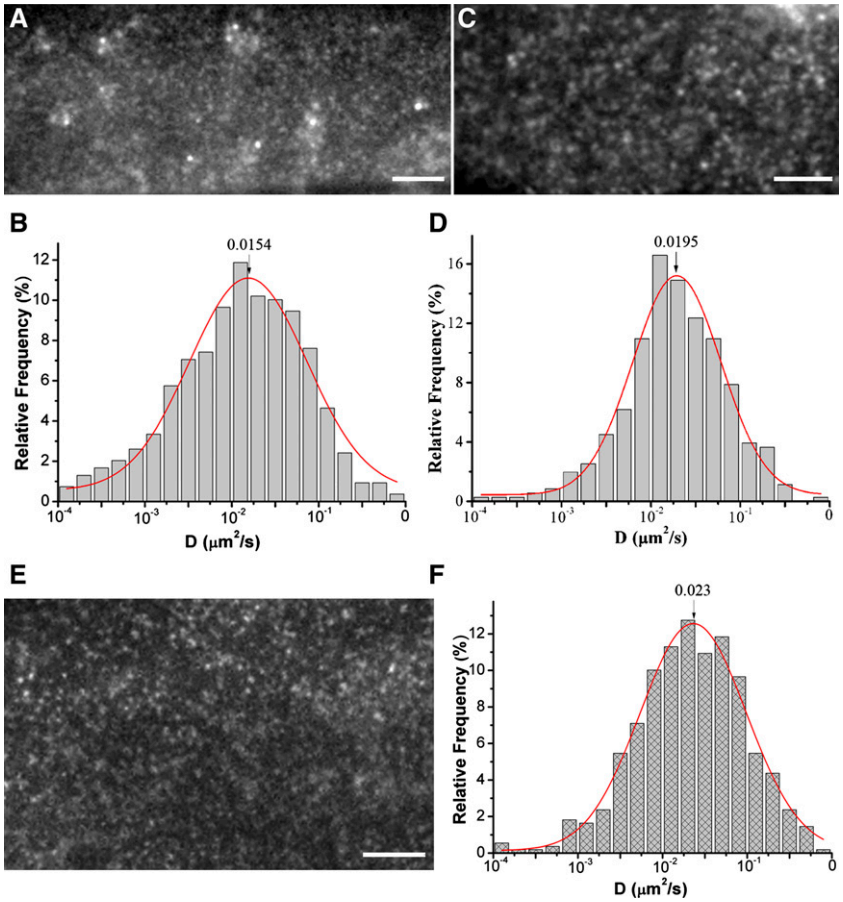

Figure 5. Interruption of the Clathrin-Dependent Pathway Affects GFP-RbohD Foci Dynamics at the Plasma Membrane.

(A) VA-TIRFM image of epidermal cells fluorescently labeled with GFP-RbohD and treated with TyrA23. Bar = 5 μm.
(B) Distribution of GFP-RbohD diffusion coefficients on the epidermal cell plasma membrane in the presence of TyrA23 (*n* = 475 spots).
(C) VA-TIRFM image of GFP-RbohD in the *chc2-1* mutant. Bar = 5 μm.
(D) Distribution of GFP-RbohD diffusion coefficients on the epidermal cell plasma membrane in the *chc2-1* mutant (*n* = 430 spots).
(E) VA-TIRFM image of epidermal cells fluorescently labeled with GFP-RbohD and treated with TyrA51. Bar = 5 μm.
(F) Distribution of GFP-RbohD diffusion coefficients on the epidermal cell plasma membrane in the presence of TyrA51 (*n* = 612 spots).
[See online article for color version of this figure.]

clear spots at the plasma membrane, some of which were overlaid when the two channels were merged, suggesting partial colocalization (Figures 8A to 8C). To evaluate the relative contribution of membrane microdomains to the regulation of mobility of RbohD, we also analyzed the codiffusion of mCherry-RbohD and GFP-Flot1 (Figures 8D and 8E). We found that mCherry-RbohD and GFP-Flot1 colocalization disappeared gradually with increasing distance from the focus. This result eliminated the possibility that colocalization represented simple, random overlap of highly dense spots at the membrane. The trajectories of these spots further showed that mCherry-RbohD and GFP-Flot1 codiffused at the plasma membrane for 8 s (Figure 8F) at a distance of within 120 nm. We also evaluated the degree of colocalization using the PPI method. Figure 8G depicts a 3D cross-correlation plot of Figure 8D as a function of pixel shift, a sharp peak at the zero pixel shift that decayed abruptly upon movement of the image in the *x* and *y* axes, indicating their specific colocalization. The mean PPI was 0.26 ± 0.06. We also detected lateral mobility of GFP-RbohD spots in the *Flot1* artificial microRNA (amiRNA) knockdown line, which shows a reduction in *Flot1* transcript level and growth defects (Li et al., 2012). As shown in Figure 8H, the diffusion coefficient of GFP-RbohD spots shifted to lower values, and $\hat{G}$ was $2.0 \pm 0.19 \times 10^{-2}$ $\mu m^2/s$, further confirming that the lateral diffusion of RbohD depends on the membrane microdomain. Additionally, to investigate the role of Ca^{2+} and phosphorylation in the colocalization of RbohD and Flot1, we treated seedlings coexpressing mCherry-RbohD and GFP-Flot1 with ionomycin or calyculin A and then imaged them with VA-TIRFM. The results showed that the mean protein proximity value increased to 0.42 ± 0.09 ($P < 0.01$) and 0.35 ± 0.04 ($P < 0.05$) (*n* = 10 cells) after ionomycin and calyculin A treatments, respectively, indicating that both Ca^{2+} and phosphorylation enhanced mCherry-RbohD and GFP-Flot1 colocalization.

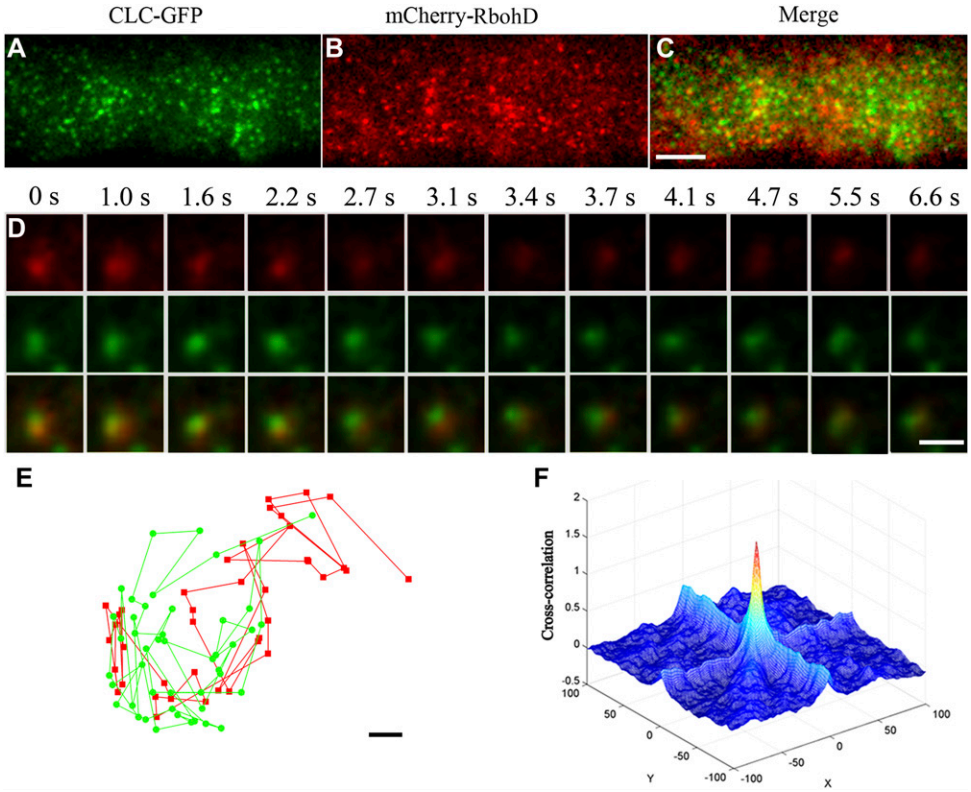

Figure 6. CLC-GFP and mCherry-RbohD Foci Colocalized at the Plasma Membrane.

(A) to **(C)** Seedlings expressing CLC-GFP and mCherry-RbohD imaged by VA-TIRFM.
(D) Corresponding mCherry-RbohD (top), CLC-GFP (middle), and merged (bottom) images for which the intensities were measured are shown below the time points indicated.
(E) The trajectories of colocalized spots of mCherry-RbohD and CLC-GFP. The mCherry-RbohD spot and CLC-GFP spot diffused together on the plasma membrane and kept their distances within ~100 nm.
(F) CLC-GFP and mCherry-RbohD 3D cross-correlation plot as a function of pixel shift.
Bars = 5 μm in **(A)** to **(C)**, 1 μm in **(D)**, and 0.05 μm **(E)**.

Clathrin- and Membrane Microdomain–Mediated Pathways Cooperatively Regulate Endocytosis of RbohD under Salt Stress

RbohD plays a key role in the response to salt stress, and salt acclimation requires the ROS generated by RbohD (Xie et al., 2011; Ma et al., 2012). Therefore, we used FM4-64 to investigate the dynamics and endocytic pathways of GFP-RbohD under salt stress. Under control conditions, GFP-RbohD localizes homogenously with FM4-64 at the plasma membrane, as assessed by confocal microscopy (Figure 9A). Treatment with 100 mM NaCl produced a change in the distribution of GFP-RbohD and the appearance of GFP-RbohD in discrete intracellular patches labeled with FM4-64 (Figure 9B), suggesting that salt stress enhanced the endocytosis of GFP-RbohD. We then assessed the changes in dynamic partitioning of GFP-RbohD caused by NaCl treatment using VA-TIRFM. Consistent with increased endocytosis, NaCl treatment induced a decrease in the number of GFP-RbohD spots at the plasma membrane (Figure 9C), while the diffusion coefficient of the GFP-RbohD spots increased (Figure 9D; Supplemental Movie 9 and Supplemental Data Set 1), ranging from 5.9×10^{-3} to 3.1×10^{-1} $\mu m^2/s$. Also, $\hat{G}$ was $4.84 \pm 0.38 \times 10^{-2}$ $\mu m^2/s$ after treatment with 100 mM NaCl versus $2.26 \pm 0.19 \times 10^{-2}$ $\mu m^2/s$ under control conditions. In seedlings treated with NaCl and mβCD or NaCl and TyrA23, the $\hat{G}$ of GFP-RbohD decreased to $3.0 \pm 0.10 \times 10^{-2}$ $\mu m^2/s$ and $1.79 \pm 0.11 \times 10^{-2}$ $\mu m^2/s$, respectively (Figures 9E and 9F; Supplemental Movies 10 and 11 and Supplemental Data Set 1), suggesting that NaCl treatment increased the endocytosis of GFP-RbohD and that disruption of the membrane microdomains and clathrin-coated pits differentially inhibited the diffusion of GFP-RbohD. Furthermore, we analyzed the abundance of protein in the presence of salt stress using immunoblots. We found that NaCl induced the degradation of GFP-RbohD to some extent. However, wortmannin, an efficient inhibitor of protein trafficking to the plant vacuole (daSilva et al., 2005; Robinson et al., 2008), inhibited the degradation of GFP-RbohD compared with the control seedlings (Supplemental Figure 6).

To further investigate the relationship between RbohD localization and recycling at the plasma membrane, we measured the density of GFP-RbohD at the plasma membrane by FCS. This technique allows analysis of fluorescence intensity fluctuation within the focal volume of the laser beam. Stable fluorescence fluctuation indicated that no significant photobleaching effects

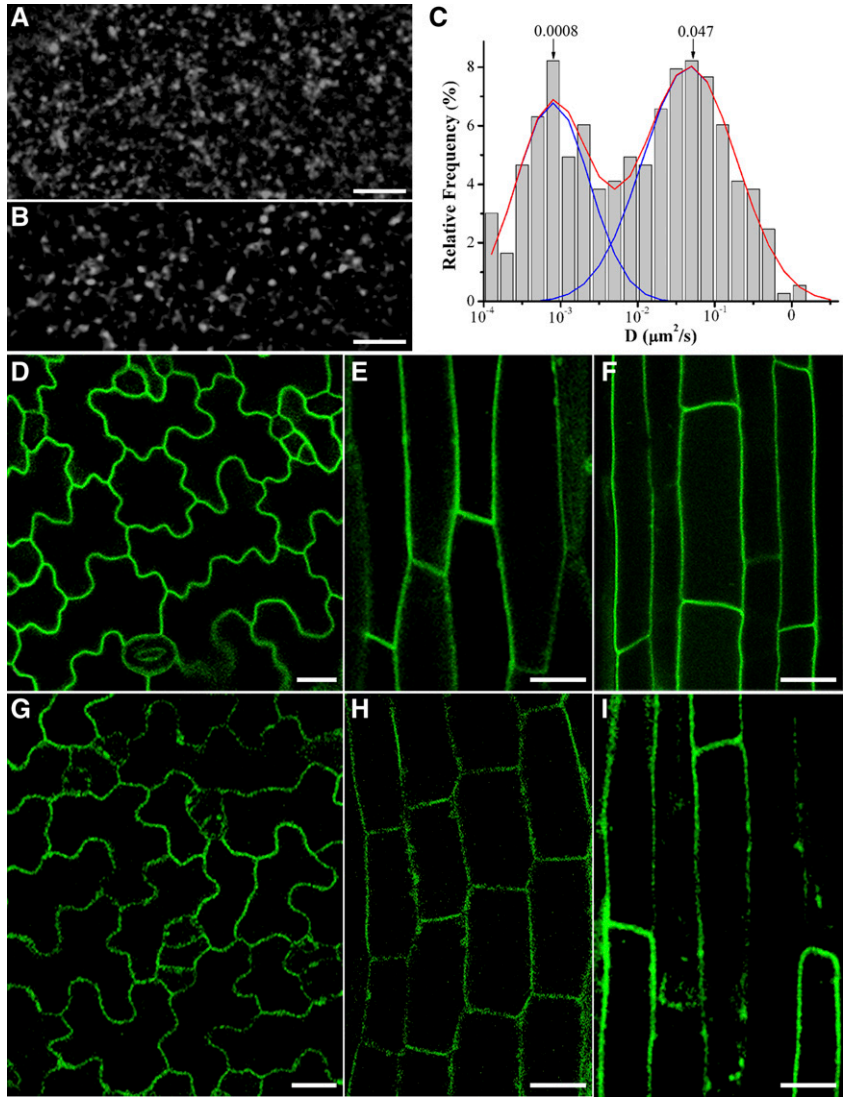

Figure 7. Effects of Sterol on the Localization and Diffusion of GFP-RbohD at the Plasma Membrane.

(A) Distribution of GFP-RbohD spots in control seedlings.
(B) Effect of mβCD on the distribution pattern of GFP-RbohD at the plasma membrane.
(C) Distribution of GFP-RbohD diffusion coefficients on the epidermal cell plasma membrane in the presence of mβCD (*n* = 429 spots).
(D) to **(F)** In the L*er* control, GFP-RbohD was localized principally at the plasma membrane in the leaf **(D)**, hypocotyl **(E)**, and root **(F)**.
(G) to **(I)** Confocal images of *dry2/sqe1-5* mutants showing uneven GFP-RbohD distribution at the membrane in leaf **(G)**, hypocotyl **(H)**, and root **(I)**.
Bars = 5 μm in **(A)** and **(B)** and 20 μm in **(D)** to **(I)**.

occurred during the detection time. The mean density of GFP-RbohD was 29.84 ± 4.12 molecules/μm^2 in control seedlings. Treatment with TyrA23 and mβCD caused an increase of the GFP-RbohD density to 49.97 ± 6.43 and 35.16 ± 4.87 molecules/μm^2, respectively, suggesting that clathrin-dependent endocytosis is the main pathway for internalization of GFP-RbohD. In the presence of NaCl, GFP-RbohD density decreased to 17.43 ± 3.59 molecules/μm^2, further supporting the NaCl-induced internalization of GFP-RbohD. However, when seedlings were pretreated with TyrA23 or mβCD before NaCl treatment, GFP-RbohD density increased to 40.95 ± 4.65 and 30.34 ± 3.23 molecules/μm^2, respectively, indicating that the disruption of these endocytic pathways differentially inhibited NaCl-induced GFP-RbohD internalization (Supplemental Figure 7A).

To further evaluate whether the interactions of mCherry-RbohD with clathrin-dependent endocytosis or membrane microdomain protein Flot1 changed under different conditions, we applied dual-color FCCS to seedlings coexpressing mCherry-RbohD and either CLC-GFP or GFP-Flot1. FCCS facilitates quantitative investigation of protein interactions in live cells (Bacia and Schwille, 2007), in which fluctuations of two different fluorescence signals are recorded simultaneously and analyzed using a cross-correlation function (Muto et al., 2009). The relative cross-correlation amplitude of seedlings

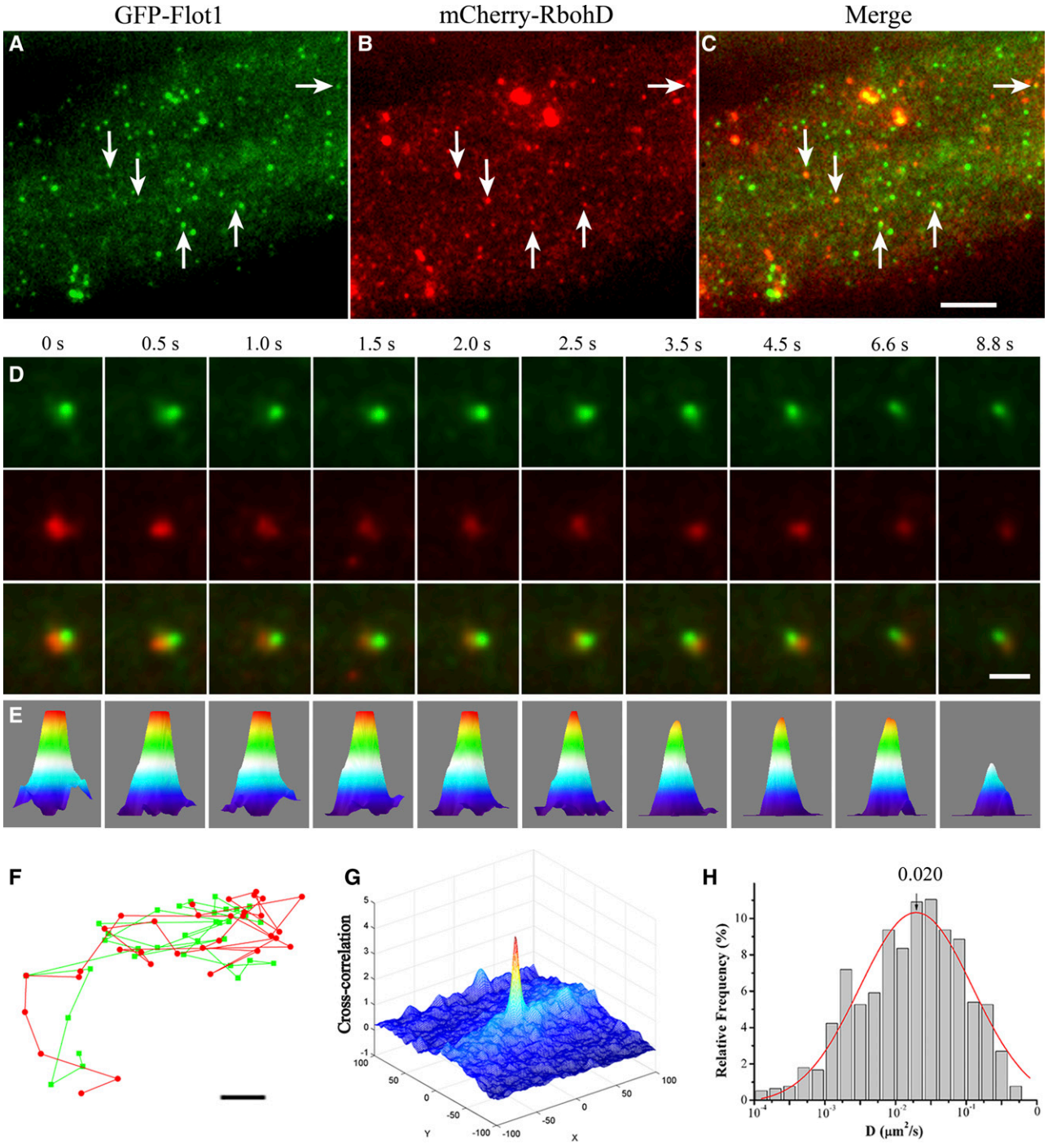

Figure 8. Colocalization of mCherry-RbohD and GFP-Flot1 Foci at the Plasma Membrane.

(A) to **(C)** Epidermal cells expressing mCherry-RbohD and GFP-Flot1 imaged by VA-TIRFM. Foci with both GFP and mCherry fluorescence are indicated (white arrows).

(D) Intensity profiles of GFP (green) and mCherry (red) fluorescence in overlapping foci. Corresponding GFP-Flot1 (top), mCherry-RbohD (middle), and merged (bottom) images for which the intensities were measured are shown below the time points indicated.

(E) Three-dimensional luminance plots of the spots in the bottom row in **(D)**.

(F) The trajectories of colocalized spots of mCherry-RbohD and GFP-Flot1. The mCherry-RbohD spot and GFP-Flot1 spot diffused together on the plasma membrane and kept their distances within ~120 nm.

(G) mCherry-RbohD and GFP-Flot1 3D cross-correlation plot as a function of pixel shift.

(H) Distribution of GFP-RbohD diffusion coefficients in *Flot1* amiRNA mutants (n = 589 spots).

Bars = 5 μm in **(A)** to **(C)**, 1 μm in **(D)**, and 0.05 μm **(F)**.

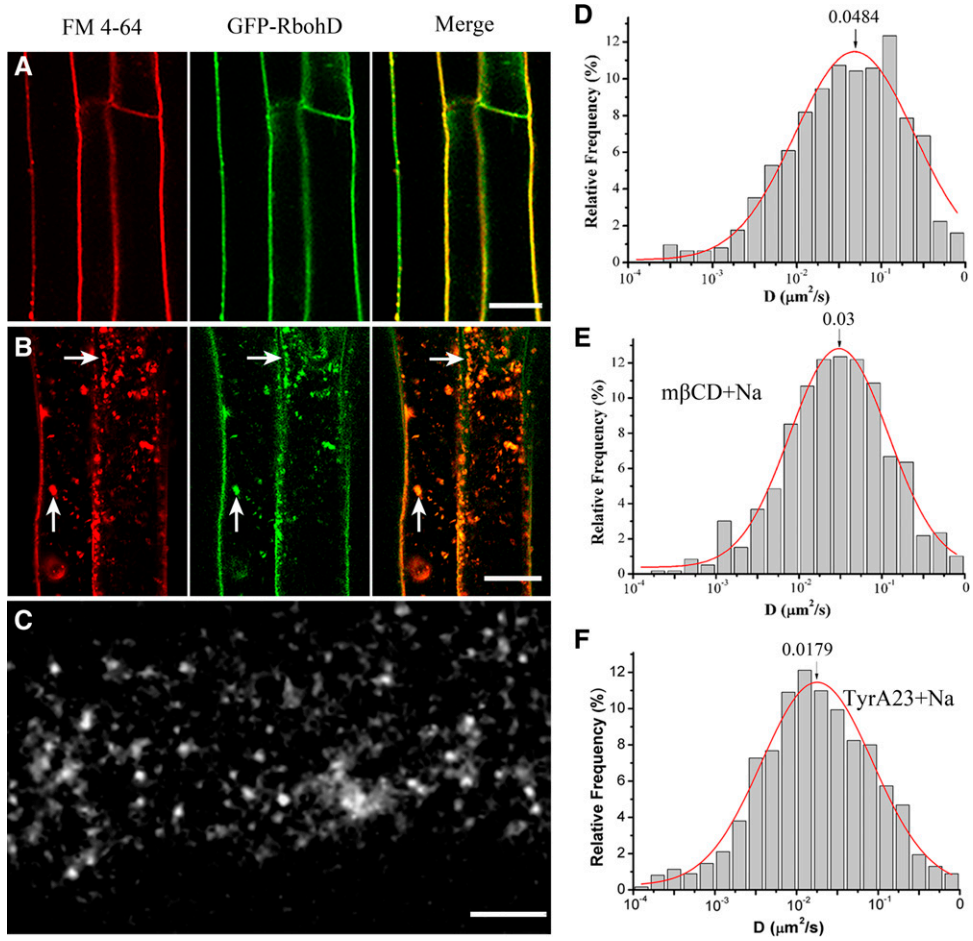

Figure 9. Effects of NaCl Treatment on the Localization and Dynamic Behavior of GFP-RbohD.

(A) In control cells, after pretreatment with cycloheximide (50 μM) for 30 min, distinct GFP-RbohD and FM4-64 colocalization was observed at the plasma membrane; a few spots were found in the cytoplasm. Bar = 20 μm.
(B) NaCl treatment led to the uneven distribution of GFP-RbohD at the plasma membrane. After pretreatment with cycloheximide (50 μM) for 30 min, GFP-RbohD colocalized with FM4-64 in the cytoplasm upon exposure to NaCl. White arrows indicate cytoplasmic fluorescence clusters. Bar = 20 μm.
(C) Dynamic partitioning of GFP-RbohD on the plasma membrane of epidermal cells in the presence of NaCl. Bar = 5 μm.
(D) Distribution of GFP-RbohD diffusion coefficients on the epidermal cell plasma membrane under NaCl stimulation (n = 633 spots).
(E) Distribution of diffusion coefficients upon treatment with mβCD prior to exposure to NaCl (n = 491 spots).
(F) Distribution of diffusion coefficients after pretreatment with TyrA23 prior to exposure to NaCl (n = 475 spots).

coexpressing mCherry-RbohD and CLC-GFP was 0.52 ± 0.09 (n = 30), while that of seedlings coexpressing mCherry-RbohD and GFP-Flot1 was 0.41 ± 0.12 (n = 30; Supplemental Figure 7B). After NaCl treatment, the cross-correlation of mCherry-RbohD with CLC-GFP increased to 0.61 ± 0.07 (a 17% increase) while that with GFP-Flot1 increased to 0.54 ± 0.1 (a 32% increase), both showing significant differences. Overall, these results support the notion that GFP-RbohD is internalized via both clathrin-dependent and membrane raft–associated pathways.

DISCUSSION

The plasma membrane, which defines the boundary of cells, plays crucial roles in signal transduction as the platform for early signaling events. In this respect, single-particle approaches provide useful tools for tracking the dynamics of proteins in living cells (Konopka and Bednarek, 2008; Fan et al., 2013; Li et al., 2013). Compared with conventional fluorescence microscopy, single-particle imaging can be used to quantitatively investigate the spatial and temporal molecular heterogeneity of membrane proteins and monitor the effects of molecular interactions (Groves et al., 2008; Reck-Peterson et al., 2010). In this study, we used our automated detection and tracking assay (Wan et al., 2011) to evaluate the spatial distribution and complex dynamics of GFP-RbohD spots in living *Arabidopsis* cells at the single-particle level using VA-TIRFM, a wide-field imaging technique with a high signal-to-noise ratio and high temporal resolution (Stock et al., 2003; Wagner et al., 2012). Our findings offer new insights into the regulation of the activity of RbohD.

Lateral mobility provides an important indicator of membrane protein state and local environment, which can affect protein mobility (Xiao et al., 2008a; Knight et al., 2010). Studies tracking the lateral diffusion of proteins at the plasma membrane have used several techniques, including fluorescence recovery after photobleaching. However, these methods cannot determine the transition kinetics of diffusion mobility. In this study, we evaluated the lateral diffusion of GFP-RbohD spots at the plasma membrane using VA-TIRFM and single-particle tracking. The results showed that GFP-RbohD organized into discreet, dynamic spots at the cell cortex. We found that GFP-RbohD particles at the plasma membrane have different diffusion coefficients, characterized by a unimodal distribution with a peak value of almost $2.26 \pm 0.19 \times 10^{-2}$ $\mu m^2/s$. Additionally, we found that the number of bleaching steps ranged from one to two, indicating that GFP-RbohD at the plasma membrane exists in multiple oligomeric forms, including monomers and dimers. This is consistent with previous crystallographic studies (Oda et al., 2010), which reported that the active conformation of OsRbohB is a dimer and that monomers interact via their terminal cytoplasmic domains. The dispersion of the diffusion coefficient distribution and the different oligomeric states suggest that GFP-RbohD is highly mobile and heterogeneously distributed at the plasma membrane.

RbohD function has been implicated in plant defense responses. However, the detailed activation mechanism of RbohD has remained unclear. Kazmierczak and Lipniacki (2009) found that the diffusion coefficient was related to the activation of kinase. Thus, we next investigated the relationship between the mobility and activation of RbohD. Using VA-TIRFM, we found that as a specific inhibitor of NADPH, DPI induced a decrease in the diffusion coefficient, from $2.26 \pm 0.19 \times 10^{-2}$ $\mu m^2/s$ in the control to $1.68 \pm 0.08 \times 10^{-2}$ $\mu m^2/s$, suggesting that the low lateral mobility induced by DPI may be attributable to its binding to the redox center of flavoproteins. In transgenic seedlings treated with ionomycin and calyculin A, the diffusion coefficients increased from $2.26 \pm 0.19 \times 10^{-2}$ $\mu m^2/s$ in the control to $4.1 \pm 0.3 \times 10^{-2}$ and $3.49 \pm 0.13 \times 10^{-2}$ $\mu m^2/s$, respectively. Because Ca^{2+} binding to its EF-hand region mediates the ionomycin-induced activation of RbohD (Ogasawara et al., 2008), it is likely that the faster diffusion of GFP-RbohD after stimulation was due largely to a Ca^{2+}- or phosphorylation-induced conformational change in RbohD. It is important to note that ionomycin and calyculin A increased the percentage of the dimer significantly, from 28 to 76% ($P < 0.01$) and 55% ($P < 0.05$), respectively, indicating that RbohD formed dimers upon activation by Ca^{2+} or phosphorylation. These results indicate that the monomer-dimer transitions at the plasma membrane may represent an essential aspect of NADPH oxidase function in redox signaling. Furthermore, parallel experiments with the transgenic seedlings expressing GFP-Iti6a, an internal marker of the plasma membrane, showed that neither the inhibitor, nor the activator of the NADPH oxidase affected the dynamics and intensity of GFP-Iti6a spots, indicating that these effectors of NADPH oxidase specifically affect GFP-RbohD. We also note that in response to ABA and flg22, both the intensity and mobility of GFP-RbohD spots increased. The diffusion coefficient of GFP-RbohD was $5.32 \pm 0.29 \times 10^{-2}$ $\mu m^2/s$ and $4.65 \pm 0.41 \times 10^{-2}$ $\mu m^2/s$ in the presence of ABA and flg22, respectively. These results demonstrate that the dynamics and clustering of RbohD may play an important role in regulating its activity and function.

Endocytotic turnover affects membrane protein turnover and the activity of signaling pathways (Takeda et al., 2008). Maintenance of RbohC in the plasma membrane requires vesicle trafficking and phagocyte NADPH oxidase can be internalized from the plasma membrane by endocytosis (Takeda et al., 2008; Oakley et al., 2009). However, whether the localization of RbohD requires endocytosis and the contribution of the different endocytic pathways remain unclear. In this study, we found that GFP-RbohD colocalized with FM4-64, the membrane marker, at the plasma membrane. To investigate the endocytosis of GFP-RbohD, we inhibited endocytic recycling using the fungal toxin BFA and found that both GFP-RbohD and FM4-64 accumulated in the BFA compartment. Salt stress also significantly increased internalization of GFP-RbohD. This is consistent with a previous study (Leshem et al., 2007), which reported that salt stress can induce the endocytosis of the plasma membrane and the intracellular production of ROS. The authors of this study speculated that the subcellular localization of ROS depends on vesicle trafficking, according to the binding of differentially phosphorylated PIs. Internalized RbohD may result in the generation of ROS within endosomes, which may affect ROS-dependent signal transduction through the subcellular modifications of signaling proteins. Immunoblot experiments were further performed to test the GFP-RbohD protein content after treatment with NaCl. The results confirmed that some GFP-RbohD was transported to the vacuole for degradation in the presence of NaCl. These results provide strong evidence that the activity of RbohD at the plasma membrane depends on vesicle trafficking and the constitutive internalization of GFP-RbohD. Also, plants may use endocytosis to regulate the surface localization of RbohD protein and control the activation of redox signaling pathways.

Clathrin-mediated endocytosis is the main endocytic pathway regulating the steady state levels of numerous membrane proteins (Dhonukshe et al., 2007). For instance, continuous endocytosis of the auxin efflux carriers PIN1 and PIN2 requires clathrin (Dhonukshe et al., 2007). Although the existence of clathrin-mediated endocytosis in plants is now widely accepted, the molecular machinery responsible for the regulated uptake of membrane and endocytic cargoes is less well understood. Our data provide evidence that the internalization of GFP-RbohD also depends on clathrin. Treatment with TyrA23, which can disrupt clathrin-dependent endocytosis by specifically preventing the interaction of cargo motifs and the μ2 subunit (Banbury et al., 2003), caused an increase in the density of GFP-RbohD and a decrease in its diffusion coefficient. Konopka et al. (2008) reported the effects of TyrA23 on the endocytic spots, showing that the size and fluorescence of DRP1C-GFP increased in the presence of TyrA23. However, TyrA51, the inactive phosphotyrosine analog of TyrA23, had no effect on the dynamics and distribution of GFP-RbohD. Moreover, mCherry-RbohD colocalized and codiffused with CLC-GFP at the plasma membrane. The PPI value of mCherry-RbohD and CLC-GFP colocalization was 0.54 ± 0.1. These results indicate that clathrin functions in the endocytosis of RbohD. Genetic evidence also supported this clathrin dependency. Using the *chc2* mutant, a homozygous knockout line of the gene encoding clathrin heavy chain (*CHC*), in which endocytosis was reduced significantly (Kitakura et al., 2011), we found that some RbohD accumulated at the plasma membrane. Similar to the *chc2* mutant, with TyrA23 treatment,

the diffusion coefficient decreased to $1.95 \pm 0.1 \times 10^{-2}$ $\mu m^2/s$. FCCS analyses showed that the relative cross-correlation amplitude of mCherry-RbohD and CLC-GFP was 0.52 ± 0.09, confirming that GFP-RbohD interacts strongly with clathrin. Taken together, our data demonstrate that the clathrin-dependent pathway plays the predominant role in RbohD internalization.

In addition to clathrin-dependent endocytosis, cells also use clathrin-independent endocytosis (Zappel and Panstruga, 2008). Men et al. (2008) reported that sterol-dependent endocytosis mediated the postcytokinetic acquisition of PIN2 auxin efflux carrier polarity in *Arabidopsis*. In animal and yeast cells, membrane microdomains form specialized regions enriched in cholesterol and glycosphingolipids and may function as sorting platforms for proteins destined for signal transduction, pathogen entry, secretion, and endocytosis (Simons and Toomre, 2000; Ikonen, 2001). Sterol-based membrane microdomains in plants also affect the polar localization of auxin efflux carriers, a major determinant of cell polarity (Willemsen et al., 2003; Dhonukshe, 2009) and a component of endocytic vesicles that accumulate in ARA6-positive endosomes (Grebe et al., 2003). In this study, we found that the size of GFP-RbohD spots increased and most of the spots were confined within small particles after treatment with mβCD, a sterol-depleting agent. Also, in the *dry2/sqe1-5* mutant, GFP-RbohD delocalized from the plasma membrane and accumulated in small cytoplasmic compartments. mCherry-RbohD colocalizes with GFP-Flot1 at the plasma membrane, further supporting that RbohD localization depends on sterol-based membrane microdomains. Protein proximity analyses revealed that in the presence of ionomycin or calyculin A, the degree of colocalization increased significantly as indicated by the high proximity index as compared with the control, suggesting that Ca^{2+} or phosphorylation led to an increase in the clustering of GFP-RbohD in membrane microdomains, where they are enzymatically activated by forming more stable and functional platforms (Simon-Plas et al., 2011).

Since membrane microdomains influence GFP-RbohD localization, we tested whether internalization of GFP-RbohD was associated with membrane microdomains. By FCS analysis, we found that mβCD treatment causes an increase in the density of GFP-RbohD, whereas the diffusion coefficients of GFP-RbohD distributed into two subpopulations: fast- and slow-diffusing spots. Furthermore, mCherry-RbohD codiffused with GFP-Flot1 in seedlings coexpressing mCherry-RbohD and GFP-Flot1, while the diffusion coefficient of GFP-RbohD decreased in the *Flot1* amiRNA line. In the presence of NaCl, the changes in the diffusion coefficients became more marked; furthermore, the density of RbohD at the membrane decreased upon mβCD treatment, similar to the effects of TyrA23. More importantly, FCCS analysis indicated that the interaction between mCherry-RbohD and GFP-Flot1 increased significantly, indicating enhancement of the membrane microdomain-associated pathway. Thus, we propose that the membrane microdomains play a role in altering the activity of this transmembrane protein by positively or negatively affecting its clustering and signal transduction.

In summary, our study provides important insights into the complex regulation of RbohD at the plasma membrane. Our results demonstrate that RbohD is heterogeneously distributed at the plasma membrane of living cells and RbohD activity closely relates to its lateral diffusion and dimerization state. Effectors of RbohD activity, like Ca^{2+} and phosphorylation treatment, induced faster diffusion and clustering of RbohD. Furthermore, clathrin and membrane microdomains synergistically affect the endocytosis of RbohD (Supplemental Figure 8), regulating RbohD activity by changing its mobility and effective amount at the plasma membrane.

METHODS

Plant Materials

Arabidopsis thaliana ecotypes Columbia-0 and Landsberg *erecta* (L*er*) were used as wild-type controls. The *dry2/sqe1-5* mutants were a generous gift from Miguel A. Botella (Universidad de Málaga), and the *rbohD* mutants were a generous gift from Miguel Angel Torres (John Innes Institute). *Flot1* amiRNA knockdown lines were developed in our laboratory (Li et al., 2012). *chc 2-1* mutants were a generous gift from Jiří Friml (Ghent University). GFP-LTi6a lines were described elsewhere (Cutler et al., 2000). Seeds were surface-sterilized and germinated on half-strength Murashige and Skoog (MS) medium in phytagar after 1 to 2 days at 4°C and grown on vertically oriented plates at 24°C under stable long-day (16-h light/8-h dark) conditions.

Plasmid Construction and Plant Transformation

The *RbohD* coding region was amplified from a cDNA library derived from seedlings of *Arabidopsis* and subcloned into the binary plant expression vector pCMBIA2300 under the control of the native promoter. The GFP sequence was cloned from pM999-GFP (kindly provided by Jianxu, National University of Singapore). The GFP-Flot1 and CLC-GFP plant expression vector was constructed as follows: *Flot1* and *CLC* were PCR amplified and subcloned into the modified pCAMBIA2300 and pCAMBIA1301 vectors, respectively. *Arabidopsis* ecotype Columbia wild-type or L*er*, the *dry2/sqe1-5* mutant, *rbohD* mutant, and *Flot1* amiRNA line were transformed with constructs for GFP-RbohD or mCherry-RbohD, using the *Agrobacterium tumefaciens*–mediated floral dip method (Clough and Bent, 1998). CLC-GFP and GFP-Flot1 plants were transformed with the constructs for mCherry-RbohD. For *chc2-1* mutant seedlings expressing GFP-RbohD, F2 lines derived from crosses between GFP-RbohD and *chc2-1* were identified. Transgenic plants were selected on solid medium (1.5% agar), half-strength MS medium containing 50 μg/mL hygromycin for CLC-GFP and GFP-Flot1, and 70 μg/mL kanamycin for GFP-RbohD and mCherry-RbohD.

Fluorescent Dyes and Inhibitor Treatments

FM4-64 (Molecular Probes) in water was applied at a 3 μM final concentration to *Arabidopsis* plants, which were then washed with medium to remove excess dye and observed immediately. TyrA23, TyrA51, BFA, calyculin A, ionomycin, K-252a, wortmannin, and CHX were used from DMSO-dissolved stock solutions. mβCD was prepared in deionized water. For drug treatment, vertically grown seedlings were incubated in half-strength MS medium containing 50 μM Tyr A23, 50 μM TyrA51, 50 μM CHX, 50 μM BFA, 10 mM mβCD, or 33 μM wortmannin before VA-TIRFM, confocal microscopy, or immunoblot analysis. ABA and flg22 were added to a final concentration of 10 μM. Incubation of *Arabidopsis* seedlings in the presence of various chemicals was performed in 24-well cell culture plates in liquid half-strength MS medium. The final DMSO concentration in all working solutions was 0.1% (v/v) or less. For VA-TIRFM analysis, inhibitor treatment was for 30 min, unless otherwise stated. For confocal imaging, 4-d-old vertically grown seedlings were transferred to half-strength MS in a 12-well culture plate. After the indicated times, seedlings were transferred to a glass slide with a small quantity of inhibitor solution and covered with a glass cover slip. For

Arabidopsis, experiments were performed in triplicate with at least 60 seedlings evaluated for each experimental condition.

Confocal Microscopy and Image Analyses

Seedlings were viewed under a confocal microscope (Carl Zeiss) using a 488-nm Ar/Kr laser line exciting GFP and FM4-64. GFP and FM4-64 emission was captured with a 500- to 525-nm slit detector setting. For plants expressing GFP and mCherry, Zeiss LSM 5 LIVE was used for colocalization analysis. GFP and mCherry were excited with 488- and 561-nm lasers, respectively (multitrack mode). Fluorescence was detected using the spectral detector set band-pass 520 to 555 (GFP) and long-pass 575 (mCherry). Images acquired were processed using Adobe Photoshop, version 7.

Single-Particle Fluorescence Imaging

The 4-d-old *Arabidopsis* control seedlings or those treated with inhibitors in a 12-well culture plate were transferred to a glass slide, covered with a cover slip, and observed under an objective-type total internal reflection fluorescence microscope. The VA-TIRFM microscope consisted of an inverted microscope (IX-71; Olympus), equipped with a laser-based TIRFM illumination module (IX2-RFAEVA-2; Olympus) and an Olympus PlanApo ×100 1.45–numerical aperture oil objective.

GFP-tagged molecules were excited by a 473-nm laser, and the laser intensity was set at 0.2 μW μm^{-2}. Fluorescence signals were collected using the objective lens and passed through two filters, a BA 510IF long-pass filter (Chroma USA) and a HQ525/50 band-pass filter (Chroma), before being detected using a back-illuminated electron-multiplying charge-coupled device (EMCCD) camera (ANDOR iXon DV897D-CS-BV; Andor Technology). For colocalization analysis, GFP and mCherry (561 nm) were excited simultaneously. The emissions were collected through high-quality filters (band-pass 525/45 and 609/54). The gain of the EMCCD camera was set at 300 throughout the single-particle imaging experiment; this setting was in the linear dynamic range of the EMCCD camera. Movies of 100 to 200 frames were acquired for each sample at a frame rate of 4 Hz.

Image Analysis, Tracking of Single Particles, and PPI Estimates

Single-particle fluorescence imaging of GFP on cover slips was performed as a control experiment. rAcGFP1 protein (Clontech) was first immobilized on cover slips using a biotin-coupled GFP antibody (Clontech) according to the method reported previously (Yao et al., 2003). Fluorescence spots of rAcGFP1 that were within the diffraction limit (3 × 3 pixels, 480 nm × 480 nm) and bleached in a single step were identified as a single GFP molecule. To analyze the bleaching steps of GFP-RbohD protein, transgenic seedlings were washed with PBS three times and fixed in 4% paraformaldehyde solution for 30 min. The regions of interest for bleaching analysis were chosen according to the method of Zhang et al. (2009). The background fluorescence was subtracted from the movie acquired from the fixed seedlings using the rolling ball method in ImageJ software (US National Institutes of Health). The time courses of the fluorescence intensity of the interest regions were extracted for bleaching analysis.

The single-particle fluorescence intensity was determined as follows. The background fluorescence was first subtracted from the movie using the rolling ball method in ImageJ software and the first frame of each movie was used for fluorescent spot (region of interest) selection. After image processing, the brightest pixel in each fluorescence spot within the diffraction-limited size of 3 × 3 pixels was determined as the center position, and a square of 3 × 3 pixels was enclosed as the region of interest to calculate the fluorescence intensity with ImageJ. Any spot with a peak pixel very close to another spot (less than three pixels) was not used in the calculation.

Analyses of the dynamic properties were according to the detection methods 2 described by Jaqaman et al. (2008). Time-lapses series of single GFP-RbohD images were taken up to 100 images. To obtain trajectories of each spots, the mean square displacement (MSD) was calculated according to the equation (Haggie and Verkman, 2008):

$$\mathrm{MSD} = (x - x_0)^2 + (y - y_0)^2$$

where x and y are the coordinates at any given time, and x_0 and y_0 are the initial coordinates. For each spot, the diffusion coefficient (*D*) was calculated by plotting MSD against time (*t*) and the slope of the first four time points in the MSD-*t* plot was used according to the equation below:

$$\mathrm{MSD}_{t\to 0} = 4Dt$$

The diffusion coefficients reported in the text correspond to the peak positions (noted as $\hat{G}$) of single or multiple Gaussian fit(s) of the *D*-histograms. The distributions of GFP-RbohD diffusion coefficients were obtained under different treatments. Those exhibiting $\hat{G} < 4.2 \times 10^{-3}$ $\mu m^2/s$ (derived by the Gaussian fitting to the data of the immobile particles in the fixed seedlings) were defined as immobile molecules. Quantification of the colocalization of RbohD and Flot1/CLC was according to the protein proximity index method, as described by Wu et al. (2010).

Immunoblot Analysis

Total proteins were extracted from transgenic GFP-RbohD lines in the *rbohD* background cultured in normal medium or subjected to a 30-min treatment of wortmannin and salt stress, respectively. The seedlings were ground to a fine power in liquid nitrogen, mixed at a 1:1 (v/v) ratio with SDS-PAGE sample buffer, heated at 95°C for 15 min, and then centrifuged at 12,000*g* for 5 min. The supernatants were separated on 8% SDS/polyacrylamide gels and transferred to a polyvinylidene fluoride membrane (Immobilon-P; Millipore) by electroblotting. Immunoblot analysis was performed with monoclonal GFP antibody (Sigma-Aldrich). Horseradish peroxidase–conjugated anti-mouse secondary antibody (Sangon Biotech) was used to detect the primary antibody, and β-tubulin was used as the reference control.

Fluorescence Correlation Spectroscopy Analysis

The density of GFP-RbohD was measured using a Leica TCS SP5 FCS microscope equipped with an in-house coupled correlator and 488-nm argon laser. After acquiring images of cells in transmitted light mode, FCS was performed in the point-scanning mode and the laser was focused on the cell plasma membrane. The principle is based on the diffusion of fluorophores into and out of the focal volume, which alters the local fluorophore concentration, leading to spontaneous fluorescence intensity fluctuation. The GFP-RbohD density of individual cell membranes was obtained by monitoring the numbers of GFP-labeled RbohD molecules. Two random locations were selected, and a 10-s autocorrelation measurement per point was performed. The density of GFP-RbohD in up to 30 cells was determined in each measurement.

For dual-color cross-correlation measurements, seedlings that express both the mCherry-RbohD and CLC-GFP/GFP-Flot1 fusion proteins were used. Also, 488- and 561-nm wavelengths were used to excite the green and red fluorophores, respectively. For quantitative evaluation, the relative cross-correlation was calculated from [*Gc*(0)/*Gr*(0)], where Gc denotes the cross-correlation function and Gr denotes the autocorrelation function of the green channel.

Accession Numbers

Sequence data from this article can be found in the Arabidopsis Genome Initiative or GenBank/EMBL databases under the following accession numbers: *RbohD* (At5g47910), *Flot1* (At5g25250), and *CLC* (At2g40060).

Supplemental Data

The following materials are available in the online version of this article.

Supplemental Figure 1. Confocal Images and VA-TIRFM Analysis of GFP-RbohD in *Arabidopsis* Seedlings.

Supplemental Figure 2. Statistical Analysis of the Fluorescence Intensities of Single GFP Molecules.

Supplemental Figure 3. Dynamic Tracking and Statistical Analysis of GFP-LTi6a at the Plasma Membrane.

Supplemental Figure 4. Effects of ABA and Flg22 on the Dynamic Behavior of GFP-RbohD Spots at the Plasma Membrane.

Supplemental Figure 5. Effects of TyrA23, TyrA51, or MβCD on GFP-RbohD Focus Size and Fluorescence Intensity at the Plasma Membrane.

Supplemental Figure 6. The Degradation Analysis of GFP-RbohD Protein by Immunoblots.

Supplemental Figure 7. FCS and FCCS Measurements under Various Conditions.

Supplemental Figure 8. Hypothetical Model Summarizing the Oligomerization States and Endocytic Pathways of *Arabidopsis* RbohD.

Supplemental Movie 1. The Movie of Dynamics of GFP-RbohD Foci under Normal Condition (13 × 36 μm).

Supplemental Movie 2. The Movie of Dynamics of GFP-RbohD Foci Treated with DPI (15 × 38 μm).

Supplemental Movie 3. The Movie of Dynamics of GFP-RbohD Foci Treated with Ionomycin (15 × 34 μm).

Supplemental Movie 4. The Movie of Dynamics of GFP-RbohD Foci Treated with Calyculin A (13 × 35 μm).

Supplemental Movie 5. The Movie of Dynamics of GFP-RbohD Foci Treated with ABA (16 × 35 μm).

Supplemental Movie 6. The Movie of Dynamics of GFP-RbohD Foci Treated with Flg22 (15 × 35 μm).

Supplemental Movie 7. The Movie of Dynamics of GFP-RbohD Foci Treated with TyrA23 (15 × 37 μm).

Supplemental Movie 8. The Movie of Dynamics of GFP-RbohD Foci Treated with MβCD (12 × 36 μm).

Supplemental Movie 9. The Movie of Dynamics of GFP-RbohD Foci in the Presence of NaCl (15 × 40 μm).

Supplemental Movie 10. The Movie of Dynamics of GFP-RbohD Foci Treated with TyrA23 in the Presence of NaCl (15 × 38 μm).

Supplemental Movie 11. The Movie of Dynamics of GFP-RbohD Foci Treated with MβCD in the Presence of NaCl (16 × 40 μm).

Supplemental Data Set 1. The Supplemental Movie Legends and the Three Images (First, Middle, and Last Frames) from the Movie.

ACKNOWLEDGMENTS

We thank Miguel Angel Torres for providing us with the *rbohD* mutants and Jiri Friml for the *chc 2-1* mutant seeds. We thank Wangxi Luo for technical assistance with VA-TIRFM. We also thank Jeff Dangl for his valuable comments on the draft of this article and Frantisek Baluska for his discussion of the article. This work was supported by the National Basic Research Program of China (973 Program 2011CB944600 and 2011CB809103), the grant from the National Natural Science Foundation of China (31121065, 31170163, and 31270224), the Program of Introducing Talents of Discipline to Universities (111 project, B13007), and the Program for Changjiang Scholars and Innovative Research Team in University (IRT13047).

AUTHOR CONTRIBUTIONS

H.H. and L.F. performed experiments, analyzed the data, and wrote the article. T.C., R.L., X.L., and Q.H. performed experiments. M.A.B. revised the article. J.X. designed the experiment and revised the article.

Received January 9, 2014; revised March 6, 2014; accepted March 26, 2014; published April 22, 2014.

REFERENCES

Bacia, K., and Schwille, P. (2007). Practical guidelines for dual-color fluorescence cross-correlation spectroscopy. Nat. Protoc. **2:** 2842–2856.

Banbury, D.N., Oakley, J.D., Sessions, R.B., and Banting, G. (2003). Tyrphostin A23 inhibits internalization of the transferrin receptor by perturbing the interaction between tyrosine motifs and the medium chain subunit of the AP-2 adaptor complex. J. Biol. Chem. **278:** 12022–12028.

Borner, G.H., Sherrier, D.J., Weimar, T., Michaelson, L.V., Hawkins, N.D., Macaskill, A., Napier, J.A., Beale, M.H., Lilley, K.S., and Dupree, P. (2005). Analysis of detergent-resistant membranes in *Arabidopsis*. Evidence for plasma membrane lipid rafts. Plant Physiol. **137:** 104–116.

Clough, S.J., and Bent, A.F. (1998). Floral dip: a simplified method for Agrobacterium-mediated transformation of *Arabidopsis thaliana*. Plant J. **16:** 735–743.

Cutler, S.R., Ehrhardt, D.W., Griffitts, J.S., and Somerville, C.R. (2000). Random GFP:cDNA fusions enable visualization of subcellular structures in cells of *Arabidopsis* at a high frequency. Proc. Natl. Acad. Sci. USA **97:** 3718–3723.

daSilva, L.L., Taylor, J.P., Hadlington, J.L., Hanton, S.L., Snowden, C.J., Fox, S.J., Foresti, O., Brandizzi, F., and Denecke, J. (2005). Receptor salvage from the prevacuolar compartment is essential for efficient vacuolar protein targeting. Plant Cell **17:** 132–148.

Dhonukshe, P. (2009). Cell polarity in plants: Linking PIN polarity generation mechanisms to morphogenic auxin gradients. Commun. Integr. Biol. **2:** 184–190.

Dhonukshe, P., Aniento, F., Hwang, I., Robinson, D.G., Mravec, J., Stierhof, Y.D., and Friml, J. (2007). Clathrin-mediated constitutive endocytosis of PIN auxin efflux carriers in *Arabidopsis*. Curr. Biol. **17:** 520–527.

Espenel, C., Margeat, E., Dosset, P., Arduise, C., Le Grimellec, C., Royer, C.A., Boucheix, C., Rubinstein, E., and Milhiet, P.E. (2008). Single-molecule analysis of CD9 dynamics and partitioning reveals multiple modes of interaction in the tetraspanin web. J. Cell Biol. **182:** 765–776.

Fan, L.S., Hao, H.Q., Xue, Y.Q., Zhang, L., Song, K., Ding, Z.J., Botella, M.A., Wang, H.Y., and Lin, J.X. (2013). Dynamic analysis of *Arabidopsis* AP2 σ subunit reveals a key role in clathrin-mediated endocytosis and plant development. Development **140:** 3826–3837.

Feraru, E., and Friml, J. (2008). PIN polar targeting. Plant Physiol. **147:** 1553–1559.

Galletti, R., Denoux, C., Gambetta, S., Dewdney, J., Ausubel, F.M., De Lorenzo, G., and Ferrari, S. (2008). The AtrbohD-mediated oxidative burst elicited by oligogalacturonides in *Arabidopsis* is dispensable for the activation of defense responses effective against *Botrytis cinerea*. Plant Physiol. **148:** 1695–1706.

Grebe, M., Xu, J., Möbius, W., Ueda, T., Nakano, A., Geuze, H.J., Rook, M.B., and Scheres, B. (2003). *Arabidopsis* sterol endocytosis involves actin-mediated trafficking via ARA6-positive early endosomes. Curr. Biol. **13:** 1378–1387.

Groom, Q.J., Torres, M.A., Fordham-Skelton, A.P., Hammond-Kosack, K.E., Robinson, N.J., and Jones, J.D. (1996). rbohA, a rice homologue of the mammalian gp91phox respiratory burst oxidase gene. Plant J. **10:** 515–522.

Groves, J.T., Parthasarathy, R., and Forstner, M.B. (2008). Fluorescence imaging of membrane dynamics. Annu. Rev. Biomed. Eng. **10:** 311–338.

Haggie, P.M., and Verkman, A.S. (2008). Monomeric CFTR in plasma membranes in live cells revealed by single molecule fluorescence imaging. J. Biol. Chem. **283:** 23510–23513.

Hopps, E., Lo Presti, R., and Caimi, G. (2009). Pathophysiology of polymorphonuclear leukocyte in arterial hypertension. Clin. Hemorheol. Microcirc. **41:** 209–218.

Ikonen, E. (2001). Roles of lipid rafts in membrane transport. Curr. Opin. Cell Biol. **13:** 470–477.

Jaqaman, K., Loerke, D., Mettlen, M., Kuwata, H., Grinstein, S., Schmid, S.L., and Danuser, G. (2008). Robust single-particle tracking in live-cell time-lapse sequences. Nat. Methods **5:** 695–702.

Ji, W., Xu, P., Li, Z., Lu, J., Liu, L., Zhan, Y., Chen, Y., Hille, B., Xu, T., and Chen, L. (2008). Functional stoichiometry of the unitary calcium-release-activated calcium channel. Proc. Natl. Acad. Sci. USA **105:** 13668–13673.

Kazmierczak, B., and Lipniacki, T. (2009). Regulation of kinase activity by diffusion and feedback. J. Theor. Biol. **259:** 291–296.

Keller, T., Damude, H.G., Werner, D., Doerner, P., Dixon, R.A., and Lamb, C. (1998). A plant homolog of the neutrophil NADPH oxidase gp91phox subunit gene encodes a plasma membrane protein with Ca^{2+} binding motifs. Plant Cell **10:** 255–266.

Kimura, S., Kaya, H., Kawarazaki, T., Hiraoka, G., Senzaki, E., Michikawa, M., and Kuchitsu, K. (2012). Protein phosphorylation is a prerequisite for the Ca^{2+}-dependent activation of *Arabidopsis* NADPH oxidases and may function as a trigger for the positive feedback regulation of Ca^{2+} and reactive oxygen species. Biochim. Biophys. Acta **1823:** 398–405.

Kitakura, S., Vanneste, S., Robert, S., Löfke, C., Teichmann, T., Tanaka, H., and Friml, J. (2011). Clathrin mediates endocytosis and polar distribution of PIN auxin transporters in *Arabidopsis*. Plant Cell **23:** 1920–1931.

Knight, J.D., Lerner, M.G., Marcano-Velázquez, J.G., Pastor, R.W., and Falke, J.J. (2010). Single molecule diffusion of membrane-bound proteins: window into lipid contacts and bilayer dynamics. Biophys. J. **99:** 2879–2887.

Konopka, C.A., Backues, S.K., and Bednarek, S.Y. (2008). Dynamics of *Arabidopsis* dynamin-related protein 1C and a clathrin light chain at the plasma membrane. Plant Cell **20:** 1363–1380.

Konopka, C.A., and Bednarek, S.Y. (2008). Variable-angle epifluorescence microscopy: a new way to look at protein dynamics in the plant cell cortex. Plant J. **53:** 186–196.

Koyama-Honda, I., Ritchie, K., Fujiwara, T., Iino, R., Murakoshi, H., Kasai, R.S., and Kusumi, A. (2005). Fluorescence imaging for monitoring the colocalization of two single molecules in living cells. Biophys. J. **88:** 2126–2136.

Leshem, Y., Seri, L., and Levine, A. (2007). Induction of phosphatidylinositol 3-kinase-mediated endocytosis by salt stress leads to intracellular production of reactive oxygen species and salt tolerance. Plant J. **51:** 185–197.

Li, R., Liu, P., Wan, Y., Chen, T., Wang, Q., Mettbach, U., Baluska, F., Samaj, J., Fang, X., Lucas, W.J., and Lin, J. (2012). A membrane microdomain-associated protein, *Arabidopsis* Flot1, is involved in a clathrin-independent endocytic pathway and is required for seedling development. Plant Cell **24:** 2105–2122.

Li, X., Luu, D.T., Maurel, C., and Lin, J. (2013). Probing plasma membrane dynamics at the single-molecule level. Trends Plant Sci. **18:** 617–624.

Li, X., Wang, X., Yang, Y., Li, R., He, Q., Fang, X., Luu, D.T., Maurel, C., and Lin, J. (2011). Single-molecule analysis of PIP2;1 dynamics and partitioning reveals multiple modes of *Arabidopsis* plasma membrane aquaporin regulation. Plant Cell **23:** 3780–3797.

Liu, P., Li, R.L., Zhang, L., Wang, Q.L., Niehaus, K., Baluska, F., Samaj, J., and Lin, J.X. (2009). Lipid microdomain polarization is required for NADPH oxidase-dependent ROS signaling in *Picea meyeri* pollen tube tip growth. Plant J. **60:** 303–313.

Ma, L., Zhang, H., Sun, L., Jiao, Y., Zhang, G., Miao, C., and Hao, F. (2012). NADPH oxidase AtrbohD and AtrbohF function in ROS-dependent regulation of Na^+/K^+ homeostasis in *Arabidopsis* under salt stress. J. Exp. Bot. **63:** 305–317.

Malinsky, J., Opekarová, M., Grossmann, G., and Tanner, W. (2013). Membrane microdomains, rafts, and detergent-resistant membranes in plants and fungi. Annu. Rev. Plant Biol. **64:** 501–529.

Mayor, S., and Pagano, R.E. (2007). Pathways of clathrin-independent endocytosis. Nat. Rev. Mol. Cell Biol. **8:** 603–612.

Men, S., Boutté, Y., Ikeda, Y., Li, X., Palme, K., Stierhof, Y.D., Hartmann, M.A., Moritz, T., and Grebe, M. (2008). Sterol-dependent endocytosis mediates post-cytokinetic acquisition of PIN2 auxin efflux carrier polarity. Nat. Cell Biol. **10:** 237–244.

Monshausen, G.B., Bibikova, T.N., Weisenseel, M.H., and Gilroy, S. (2009). Ca^{2+} regulates reactive oxygen species production and pH during mechanosensing in *Arabidopsis* roots. Plant Cell **21:** 2341–2356.

Morel, J., Claverol, S., Mongrand, S., Furt, F., Fromentin, J., Bessoule, J.J., Blein, J.P., and Simon-Plas, F. (2006). Proteomics of plant detergent-resistant membranes. Mol. Cell. Proteomics **5:** 1396–1411.

Müller, K., Carstens, A.C., Linkies, A., Torres, M.A., and Leubner-Metzger, G. (2009). The NADPH-oxidase AtrbohB plays a role in *Arabidopsis* seed after-ripening. New Phytol. **184:** 885–897.

Muto, H., Kinjo, M., and Yamamoto, K.T. (2009). Fluorescence cross-correlation spectroscopy of plant proteins. Methods Mol. Biol. **479:** 203–215.

Oakley, F.D., Smith, R.L., and Engelhardt, J.F. (2009). Lipid rafts and caveolin-1 coordinate interleukin-1beta (IL-1beta)-dependent activation of NFkappaB by controlling endocytosis of Nox2 and IL-1beta receptor 1 from the plasma membrane. J. Biol. Chem. **284:** 33255–33264.

Oda, T., Hashimoto, H., Kuwabara, N., Akashi, S., Hayashi, K., Kojima, C., Wong, H.L., Kawasaki, T., Shimamoto, K., Sato, M., and Shimizu, T. (2010). Structure of the N-terminal regulatory domain of a plant NADPH oxidase and its functional implications. J. Biol. Chem. **285:** 1435–1445.

Ogasawara, Y., et al. (2008). Synergistic activation of the *Arabidopsis* NADPH oxidase AtrbohD by Ca^{2+} and phosphorylation. J. Biol. Chem. **283:** 8885–8892.

Orr, G., Hu, D., Ozçelik, S., Opresko, L.K., Wiley, H.S., and Colson, S.D. (2005). Cholesterol dictates the freedom of EGF receptors and HER2 in the plane of the membrane. Biophys. J. **89:** 1362–1373.

Pogány, M., von Rad, U., Grün, S., Dongó, A., Pintye, A., Simoneau, P., Bahnweg, G., Kiss, L., Barna, B., and Durner, J. (2009). Dual roles of reactive oxygen species and NADPH oxidase RBOHD in an *Arabidopsis*-Alternaria pathosystem. Plant Physiol. **151:** 1459–1475.

Posé, D., Castanedo, I., Borsani, O., Nieto, B., Rosado, A., Taconnat, L., Ferrer, A., Dolan, L., Valpuesta, V., and Botella, M.A. (2009). Identification of the *Arabidopsis dry2/sqe1-5* mutant reveals a central role for sterols in drought tolerance and regulation of reactive oxygen species. Plant J. **59:** 63–76.

Reck-Peterson, S.L., Derr, N.D., and Stuurman, N. (2010). Imaging single molecular motor motility with total internal reflection fluorescence microscopy (VAEM). Cold Spring Harb. Protoc. **2010:** pdb.prot5399.

Robinson, D.G., Jiang, L.W., and Schumacher, K. (2008). The endosomal system of plants: charting new and familiar territories. Plant Physiol. **147:** 1482–1492.

Sagi, M., and Fluhr, R. (2006). Production of reactive oxygen species by plant NADPH oxidases. Plant Physiol. **141:** 336–340.

Simon-Plas, F., Perraki, A., Bayer, E., Gerbeau-Pissot, P., and Mongrand, S. (2011). An update on plant membrane rafts. Curr. Opin. Plant Biol. **14:** 642–649.

Simons, K., and Toomre, D. (2000). Lipid rafts and signal transduction. Nat. Rev. Mol. Cell Biol. **1:** 31–39.

Stock, K., Sailer, R., Strauss, W.S.L., Lyttek, M., Steiner, R., and Schneckenburger, H. (2003). Variable-angle total internal reflection fluorescence microscopy (VA-TIRFM): realization and application of a compact illumination device. J. Microsc. **211:** 19–29.

Suzuki, N., Miller, G., Morales, J., Shulaev, V., Torres, M.A., and Mittler, R. (2011). Respiratory burst oxidases: the engines of ROS signaling. Curr. Opin. Plant Biol. **14:** 691–699.

Takeda, S., Gapper, C., Kaya, H., Bell, E., Kuchitsu, K., and Dolan, L. (2008). Local positive feedback regulation determines cell shape in root hair cells. Science **319:** 1241–1244.

Torres, M.A. (2010). ROS in biotic interactions. Physiol. Plant. **138:** 414–429.

Torres, M.A., and Dangl, J.L. (2005). Functions of the respiratory burst oxidase in biotic interactions, abiotic stress and development. Curr. Opin. Plant Biol. **8:** 397–403.

Torres, M.A., Dangl, J.L., and Jones, J.D. (2002). *Arabidopsis* gp91phox homologues AtrbohD and AtrbohF are required for accumulation of reactive oxygen intermediates in the plant defense response. Proc. Natl. Acad. Sci. USA **99:** 517–522.

Torres, M.A., Onouchi, H., Hamada, S., Machida, C., Hammond-Kosack, K.E., and Jones, J.D. (1998). Six *Arabidopsis thaliana* homologues of the human respiratory burst oxidase (gp91phox). Plant J. **14:** 365–370.

Wagner, M., Weber, P., Baumann, H., and Schneckenburger, H. (2012). Nanotopology of cell adhesion upon variable-angle total internal reflection fluorescence microscopy (VA-TIRFM). J. Vis. Exp. **68:** e4133.

Wan, Y.L., Ash, W.M., III., Fan, L.S., Hao, H.Q., Kim, M.K., and Lin, J. (2011). Variable-angle total internal reflection fluorescence microscopy of intact cells of *Arabidopsis thaliana.* Plant Methods **7:** 27.

Willemsen, V., Friml, J., Grebe, M., van den Toorn, A., Palme, K., and Scheres, B. (2003). Cell polarity and PIN protein positioning in *Arabidopsis* require STEROL METHYLTRANSFERASE1 function. Plant Cell **15:** 612–625.

Wu, Y., Eghbali, M., Ou, J., Lu, R., Toro, L., and Stefani, E. (2010). Quantitative determination of spatial protein-protein correlations in fluorescence confocal microscopy. Biophys. J. **98:** 493–504.

Xiao, Z., Ma, X., Jiang, Y., Zhao, Z., Lai, B., Liao, J., Yue, J., and Fang, X. (2008a). Single-molecule study of lateral mobility of epidermal growth factor receptor 2/HER2 on activation. J. Phys. Chem. B **112:** 4140–4145.

Xiao, Z., Zhang, W., Yang, Y., Xu, L., and Fang, X. (2008b). Single-molecule diffusion study of activated EGFR implicates its endocytic pathway. Biochem. Biophys. Res. Commun. **369:** 730–734.

Xie, Y.J., Xu, S., Han, B., Wu, M.Z., Yuan, X.X., Han, Y., Gu, Q., Xu, D.K., Yang, Q., and Shen, W.B. (2011). Evidence of *Arabidopsis* salt acclimation induced by up-regulation of HY1 and the regulatory role of RbohD-derived reactive oxygen species synthesis. Plant J. **66:** 280–292.

Yao, G., Fang, X., Yokota, H., Yanagida, T., and Tan, W. (2003). Monitoring molecular beacon DNA probe hybridization at the single-molecule level. Chemistry **9:** 5686–5692.

Zappel, N.F., and Panstruga, R. (2008). Heterogeneity and lateral compartmentalization of plant plasma membranes. Curr. Opin. Plant Biol. **11:** 632–640.

Zhang, W., Jiang, Y., Wang, Q., Ma, X., Xiao, Z., Zuo, W., Fang, X., and Chen, Y.G. (2009). Single-molecule imaging reveals transforming growth factor-β-induced type II receptor dimerization. Proc. Natl. Acad. Sci. USA **106:** 15679–15683.

Zinchuk, V., Wu, Y., Grossenbacher-Zinchuk, O., and Stefani, E. (2011). Quantifying spatial correlations of fluorescent markers using enhanced background reduction with protein proximity index and correlation coefficient estimations. Nat. Protoc. **6:** 1554–1567.